Thin superconductors in a perpendicular magnetic ac field. II. Circular disk

Ernst Helmut Brandt
Max-Planck-Institut für Metallforschung, Institut für Physik, D-70506 Stuttgart, Germany
(Received 14 February 1994)

The electromagnetic response of a thin type-II superconductor disk of constant thickness d to an applied perpendicular magnetic field is calculated and compared with the response of a thin strip and of bars and cylinders in a longitudinal field. The strip and disk are characterized completely by their sheet resistivity, which may be either nonlinear and static or linear, complex, and frequency dependent. The equations of motion for the sheet current in the strip and disk are derived and discussed. Iterative and numerical-solution methods are presented that account for the infinities of the integral kernel and of the ideal screening current. The linear Ohmic response, realized during flux flow or thermally activated flux flow, is calculated for a jump in the applied field and for an ac field. Simple approximate expressions for the complex ac susceptibilities of an Ohmic strip and disk are given and compared with longitudinal geometry. The penetration of perpendicular flux into an Ohmic strip or disk is *not* a usual diffusion since a logarithmic infinity of the perpendicular-field component occurs at the edges at all times t and the sheet current always flows over the entire surface. Near the edges, the sheet current has a universal profile, with a maximum which initially penetrates with constant velocity $v = 0.77D/d$ and decreases as $1/\sqrt{t}$ ($D = \rho/\mu_0$, where ρ is the resistivity). At large times $t \gg \tau_0$ the current and magnetic moment decrease as $\exp(-t/\tau_0)$, where $\tau_0 = 0.2492\,ad/D$ for a strip with half width a and $\tau_0 = 0.1815\,ad/D$ for a disk with radius a.

I. INTRODUCTION

In a previous paper[1] (in the following quoted as Ref. 1) the theory of a superconducting or normal conducting thin strip in a perpendicular time dependent magnetic field is developed. The strip, with thickness d, half width $a \gg d$, and length $L \gg 2a$, is characterized by its sheet resistivity ρ/d, which may be arbitrarily nonlinear (current dependent) or linear (complex and frequency dependent). In superconductors, the resistivity ρ is caused by moving Abrikosov vortices which may be bound elastically to pinning centers or may depin by a strong current, by thermal activation, or by tunneling. The present paper extends this theory to thin circular disks of radius a and compares both geometries. Square and rectangular plates will be treated in a forthcoming paper (part III).

The geometry of flat specimens in a perpendicular magnetic field is realized in most experiments which measure the magnetic response of high-T_c superconductors. If the plate is sufficiently thin, $d \ll a$, the magnetic moment $\mathbf{m} = \frac{1}{2}\int \mathbf{j} \times \mathbf{r} d^3r$, the dissipated power $\int \rho j^2 d^3r$, and the magnetic field outside the specimen are determined completely by the *sheet current* $\mathbf{J}(y,z) = \int_{-d/2}^{d/2} \mathbf{j}(x,y,z)\,dx$. The distribution of the current density $\mathbf{j}(x,y,z)$ over the specimen thickness d is irrelevant for its static response. For example, the sheet current equals the jump of the tangential field $\mathbf{H}_\parallel$ at the specimen surfaces; if no parallel field is applied, one has

$$\mathbf{H}_\parallel\left(\pm\frac{d}{2},y,z\right) = \pm\frac{1}{2}\mathbf{J}(y,z)\times\hat{\mathbf{x}} \tag{1.1}$$

($\hat{\mathbf{x}}$ = unit vector normal to the surface). In the area where no perpendicular flux has penetrated because of flux pinning, this longitudinal field may establish a usual (longitudinal) Bean critical state with the flux lines oriented parallel to the surface and with, e.g.,

$$\begin{aligned} j &= 0 && \text{for } |x| < x_1\,, \\ j &= j_c && \text{for } x_1 \le |x| \le x_2\,, \\ j &= -j_c && \text{for } x_2 \le |x| \le d/2\,, \end{aligned} \tag{1.2}$$

yielding a sheet current $J = (4x_2 - 2x_1 - d)j_c$. Such a critical state will be established if $d \gg \lambda$ and $J > 2H_{c1}$ (λ = magnetic penetration depth, H_{c1} = lower critical field). In thin films or for $J < 2H_{c1}$ the current is a Meissner screening current,

$$\mathbf{j}(x,y,z) = \nabla\times\mathbf{H} = \frac{\mathbf{J}(y,z)}{2\lambda}\frac{\cosh(x/\lambda)}{\sinh(d/2\lambda)}\,, \tag{1.3}$$

which flows in two surface layers if $d \gg \lambda$ or is nearly constant if $d < \lambda$. In the area where perpendicular flux has penetrated, $H_x(y,z) \neq 0$, the current is the Meissner current (1.3) plus the current caused by the curvature of the flux lines, by the terms $\partial H_y/\partial x$ and $\partial H_z/\partial x$ in $\mathbf{j} = \nabla\times\mathbf{H}$.

For the *static nonlinear* problem, explicit analytical expressions for the current and field distributions following from the Bean assumption $j_c = \text{const}$ were obtained recently for the disk[2] and strip.[3] Also analytically solved are the similar problems of a strip with transport current[4] and with transport current and perpendicular field;[5,6] see also the numerical solutions for a strip[7] and for disks of finite thickness.[8–11]

For the *dynamic* problem, when the electric field induced by the changing magnetic flux becomes important, the current distribution $\mathbf{j}(x,y,z)$ enters the magnetic response when the frequency $\omega/2\pi$ of the applied ac field is so high that the skin depth $\delta = (2\rho/\mu_0\omega)^{1/2}$ for Ohmic resistivity, or the modulus of the complex penetration depth $\lambda_{ac} = (\rho_{ac}/i\omega\mu_0)^{1/2}$ for complex linear resistivity ρ_{ac} Refs. (12,13) [see also Eqs. (1.10) and (1.15) in Ref. 1], becomes smaller than the specimen thickness d. In the general linear response case, the current distribution is given by (1.3) with the (London or Ginzburg-Landau) penetration depth λ replaced by the complex length λ_{ac}; for Ohmic resistivity ρ one has $\lambda_{ac} = (\rho/i\omega\mu_0)^{1/2} = (1-i)\delta/2$ and $\lambda_{ac}^{-1} = (1+i)\delta^{-1}$. At large frequencies, when $\delta \ll d$, the electric field is not constant over the specimen thickness and, therefore, the derivation of the equation of motion for J presented in Sec. II is no longer valid. However, this is not disturbing since in this case the sheet current is known because the strip or disk screens the applied ac field $H_a(t)$ from its interior completely like in the Meissner state and one has $J(y,z,t) \approx J_0(y,z,t)$ with

$$J_0(y,t) = H_a(t)2y/(a^2-y^2)^{1/2} \quad \text{(strip)}, \tag{1.4}$$

$$J_0(r,t) = H_a(t)\frac{4}{\pi}r/(a^2-r^2)^{1/2} \quad \text{(disk)} \tag{1.5}$$

($r^2 = x^2+y^2$, t = time). This ideal screening limit is reached not only when $\omega \gg 2\rho/(\mu_0 d^2)$, corresponding to $\delta \ll d$, but already at lower frequencies, $\omega \gg \tau^{-1} = 2\pi\rho/(\mu_0 ad)$, both for the strip with width $2a$ Refs. (14–17) and the disk with radius a.[16,17] The correct ac sheet current $J(y,z,\omega)$ determined for the strip in Ref. 1 and for the disk below in Sec. VII then deviates from the ideal screening current (1.4) or (1.5) only near the specimen edges, up to a distance $\eta \approx a/(6\omega\tau) \approx \rho/(\mu_0\omega d)$ from the edge; cf. Eq. (7.4) and Fig. 9 of Ref. 1.

Since the ideal screening current (1.4) and (1.5) is independent of $\omega \gg \tau^{-1}$, the current distribution across the thickness enters the ac losses only via a frequency dependent complex sheet resistivity

$$\rho_s = \frac{\rho}{4\delta}\frac{\sinh(d/\delta)+\sin(d/\delta)}{\sinh^2(d/2\delta)+\sin^2(d/2\delta)}, \tag{1.6}$$

with $d/\delta = (\omega d^2\mu_0/2\rho)^{1/2}$; cf. Eq. (2.25) of Ref. 1. This gives $\rho_s \approx \rho/d$ for $\delta > d$ and $\rho_s \approx \rho/2\delta$ for $\delta \ll d$. The power dissipated in the disk in a perpendicular ac field with $\omega \gg \tau^{-1}$ is obtained by integrating $J_0(r)^2\rho_s d^2$ over the disk area. This yields

$$P_{\text{disk}} = \frac{16}{\pi}\langle H_a(t)^2\rangle a^2\rho_s \ln\frac{a}{2e\Delta}, \tag{1.7}$$

where $\langle\cdots\rangle$ means time average and the diverging integral over $J_0(r)^2$ was cut off at $r = a-\Delta$. For $\tau^{-1} \ll \omega < 2\rho/(\mu_0 d^2)$ the cutoff width Δ is obtained in Sec. VI below yielding

$$P_{\text{disk}} = \frac{16}{\pi}\langle H_a(t)^2\rangle\frac{\rho a^2}{d}\ln(11.3\,\omega\tau). \tag{1.8}$$

Comparing this with the losses of a strip with length $L \gg a$ in the same frequency range, Eqs. (2.31), (5.7), and (6.3) of Ref. 1,

$$P_{\text{strip}} = 2\langle H_a(t)^2\rangle\frac{\rho aL}{d}\ln(16.2\,\omega\tau), \tag{1.9}$$

we see that the losses of a disk formally equal the losses of a strip of length $L \approx 8a/\pi$. The losses of short strips and squares are dealt with in the forthcoming part III.

The organization of the paper is as follows. In Sec. II the equations for the magnetic field and sheet current in strips and disks and the four integral kernels occurring in these equations are presented. A formal solution and limiting expressions for the ac susceptibility at low and high frequencies are given in Sec. III. An effective method to evaluate integrals with singular kernels and solve these integral equations numerically is developed in Sec. IV. As an example, the current and field and the relaxing magnetic moment, induced in an Ohmic disk by a jump in the applied perpendicular field, are calculated in Secs. V and VI. For comparison, Sec. VI gives also the magnetic moment of Ohmic slabs, cylinders, and bars with rectangular or square cross section in parallel field and discusses its relaxation at short and long times. Fourier transforming these magnetic moments one obtains the complex ac susceptibilities in Sec. VIII. The ac sheet current and magnetic field for the strip and disk are given in Sec. VII. Finally, the results are discussed and summarized in Sec. IX.

II. STRIP AND DISK GEOMETRY

In this section the equations for the sheet current and magnetic field in a thin strip and circular disk are derived and compared. As in Ref. 1, the strip or disk occupy the volume $|x| \le d/2$, $|y| \le a$, $|z| \le L/2$, or $r = (y^2+z^2)^{1/2} \le a$, Fig. 1. If the sheet current $J(y)$ (chosen along $-z$) or $J(r)$ (circling clockwise) is known, the perpendicular magnetic field in the yz plane, $H_x(y,z) = H(y)$ or $H(r)$, follows from Ampère's law, which for the strip and the disk in a constant perpendicular field H_a explicitly reads (the integrals have to be taken in the sense of Cauchy's principal value)

$$H(y) = H_a + \frac{1}{2\pi}\int_0^a J(u)\Big(\frac{1}{y-u} - \frac{1}{y+u}\Big)\,du, \tag{2.1}$$

$$H(r) = H_a + \frac{1}{2\pi}\int_0^a J(u)\Big(\frac{E(k)}{r-u} - \frac{K(k)}{r+u}\Big)\,du, \tag{2.2}$$

with $k = (4ru)^{1/2}/(r+u)$. In (2.1) the symmetry $J(-y) = -J(y)$ of the induced current was used. In (2.2) the complete elliptic integrals $E(k)$ and $K(k)$ originate from integration over the angle $\phi = \arctan(z/y)$. Note the similarity of Eqs. (2.1) and (2.2). The integral kernels in (2.1) and (2.2) also look very similar (Fig. 2)

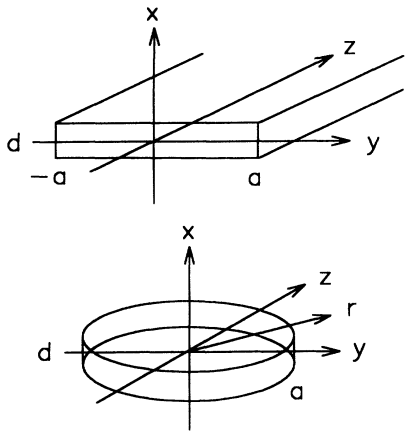

FIG. 1. Strip (top) and circular disk (bottom) in transversal magnetic field along x. d = thickness, a = half width of the strip or radius of the disk.

and may be written as

$$\frac{1}{y-u}-\frac{1}{y+u}=S(y,u)=\frac{2u}{y^2-u^2}\,, \tag{2.3}$$

$$\frac{E(k)}{r-u}-\frac{K(k)}{r+u}=P(r,u)=-\frac{1}{u}p\left(\frac{r}{u}\right), \tag{2.4}$$

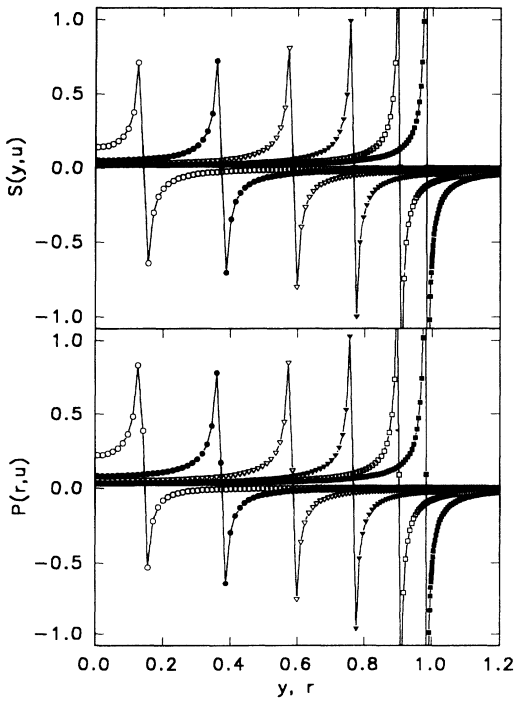

FIG. 2. The integral kernels $S(y,u)$ (2.3) for the strip and $P(r,u)$ (2.4) for the disk occurring in Eqs. (2.1), (2.2) and (4.11), (4.12). Plotted are the functions (matrices) (4.5), (4.6) with $N = 100$ and with substitution (4.1) for $i = 10$, 26, 42, 58, 74, and 90, corresponding to $u = 0.142$, 0.374, 0.587, 0.767, 0.904, and 0.984, as symbols connected by straight lines. Note the similarity of these two kernels.

$$p\,(v)=\frac{E(k)}{1-v}+\frac{K(k)}{1+v},\quad k^2=\frac{4v}{(1+v)^2}\,. \tag{2.5}$$

The equation of motion for the sheet current is derived as follows. When the magnetic flux $\phi(u) = \mu_0 L\int_0^y H(u)du$ or $\phi(r) = 2\pi\mu_0\int_0^r H(u)u\,du$ threading part of the strip or disk varies with time, it induces an electric field $E(y,t) = \dot\phi(y,t)/L$ or $E(r,t) = \dot\phi(r,t)/2\pi r$ along the boundary of this area (the dot denotes $\partial/\partial t$). Inserting here Eqs. (2.1) and (2.2) one gets the integro-differential equations for $J(y,t)$ (strip) and $J(r,t)$ (disk),

$$J(y,t)=\tau\left[2\pi y\dot H_a(t)+\int_0^1 \dot J(u,t)\,K(y,u)\,du\right], \tag{2.6}$$

$$J(r,t)\;=\;\tau\left[\pi r\dot H_a(t)+\int_0^1 \dot J(u,t)\,Q(r,u)\,du\right], \tag{2.7}$$

with the relaxation time[17]

$$\tau=\mu_0 ad/(2\pi\rho)\,. \tag{2.8}$$

In Eqs. (2.6) and (2.7) the strip half width or disk radius a is chosen as unit length and the integral kernels are

$$K(y,u)=\int_0^y S(y',u)\,dy'=\ln\left|\frac{y-u}{y+u}\right|, \tag{2.9}$$

$$Q(r,u)=\frac{1}{r}\int_0^r P(r',u)\,r'\,dr'=-q\left(\frac{r}{u}\right), \tag{2.10}$$

$$q\,(v)=\frac{1}{v}\int_0^v p\,(w)\,w\,dw\,. \tag{2.11}$$

The equations of motion (2.6) and (2.7) and the integral kernels (Fig. 3) look similar. They describe "nonlocal diffusion" of the sheet current, with the nonlocality originating from the geometry and the diffusive character from the Maxwell equations. If a nonlinear resistivity is inserted, these equations describe the flux creep in a strip or disk, which in this perpendicular geometry is a *nonlinear nonlocal diffusion.*

The universal functions $p\,(v)$ (2.5) and $q\,(v)$ (2.11) (Fig. 4) are defined in the interval $0 \le v \le \infty$ and have the following expansions for $v \ll 1$, $v \gg 1$, and $v \approx 1$:

$$p\,(v)\approx\pi+\frac{3\pi}{4}v^2,\qquad q\,(v)\approx\frac{\pi}{2}v+\frac{3\pi}{16}v^3\,, \tag{2.12}$$

$$p\,(v)\approx-\frac{\pi}{2v^3}-\frac{9\pi}{16v^5},\quad q\,(v)\approx\frac{\pi}{2v^2}+\frac{3\pi}{16v^4}\,, \tag{2.13}$$

$$p\,(v)\approx-\frac{1}{v-1}+\ln\frac{4}{|v-1|}+0.4574(1-v)\,, \tag{2.14}$$

$$q\,(v)\approx\ln\frac{1}{|v-1|}+0.07944+(v-1)\ln\frac{4e}{|v-1|}\,. \tag{2.15}$$

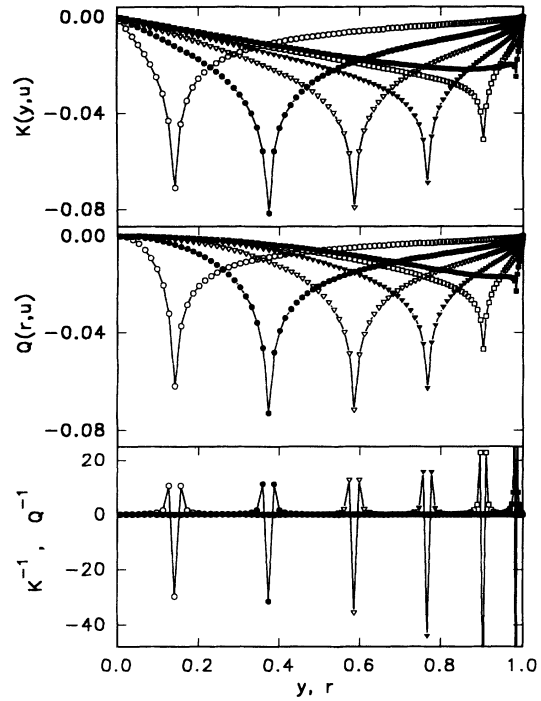

FIG. 3. The integral kernels $K(y,u)$ (2.9), (4.7) for the strip and $Q(r,u)$ (2.10), (4.8) for the disk which occur in Eqs. (2.6), (2.7) and (4.13), (4.14), plotted for the same values $u = 0.142$, 0.374, 0.587, 0.767, 0.904, and 0.984 used in Fig. 2 with $N = 100$ and the substitution (4.1). In the depicted discrete functions the logarithmic infinities are replaced by the finite values P_{jj} (4.7) and Q_{jj} (4.8). Also shown are the inverted matrices $K^{-1}(y,u)$ and $Q^{-1}(r,u)$ required in Eqs. (4.15), (4.16). The two inverted kernels coincide within line thickness. Their zigzag shape indicates that K^{-1} and Q^{-1} approximately pick out the second spatial derivative of J in (4.15), (4.16).

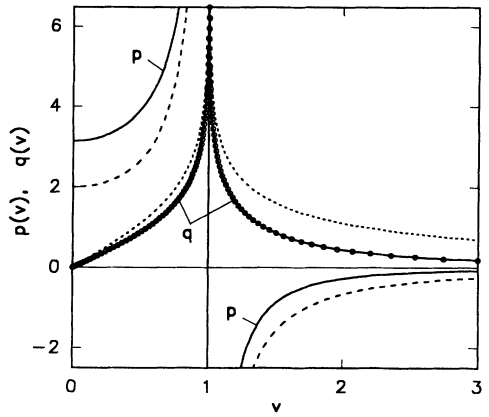

FIG. 4. The tabulated functions $p(v)$ (2.5) and $q(v)$ (2.11) from which the integral kernels for the disk are interpolated as explained in the Appendix. The nonequidistant tabulation points ($N = 80$) are indicated by the circles along $q(v)$. The dashed curves give the corresponding functions $\tilde{p}(v) = 2/(1-v^2)$ and $\tilde{q}(v) = \ln|(v+1)/(v-1)|$ from which the integral kernels for the strip may be calculated.

The functions $p(v)$ and $q(v)$ may be tabulated and integrated with high precision by a method which accounts for their infinities at $v = 1$ (Appendix).

Equations (2.6) and (2.7) are very general. They apply also when d and ρ depend on y or r (if the cross section is not rectangular, e.g., elliptical) and when the specimen is inhomogeneous or when ρ depends on the spatially varying flux density or current density. In this case the constant τ is replaced by $\tau(y)$ or $\tau(r)$. A possible nonlinearity of $\rho(T,B,J)$ is fully accounted for in Eqs. (2.6) and (2.7), which may thus be used to calculate flux creep by inserting some model resistivity, say, $\rho(J) = \exp(J/J_1)$ or $\rho(J) = \exp(-J_2/J)$, where J_1 and J_2 are constants. The model $\rho(J < J_c) = 0$, $\rho(J \geq J_c) =$ const yields the Bean critical states derived for perpendicular geometry in Refs. 2–7.

In the case of linear resistivity, a possible dispersion of $\rho = \rho_{ac}(\omega)$ is not accounted for in the time dependent formulation (2.6) and (2.7). In this case the frequency dependent formulation is appropriate. Writing $H_a(t) = H_0 \exp(i\omega t)$, and $J(y,t) = J(y)\exp(i\omega t)$ or $J(r,t) = J(r)\exp(i\omega t)$, one gets the integral equations for the complex amplitude of the sheet current in a strip or disk,

$$J(y) = i\omega\tau(\omega)\left[2\pi y H_0 + \int_0^1 J(u)\,K(y,u)\,du\right], \quad (2.16)$$

$$J(r) = i\omega\tau(\omega)\left[\pi r H_0 + \int_0^1 J(u)\,Q(r,u)\,du\right], \quad (2.17)$$

with $\tau(\omega) = \mu_0 ad/[2\pi\rho_{ac}(\omega)]$. The solutions $J(y,t)$ or $J(r,t)$ for arbitrary time dependence of $H_a(t)$ are obtained from (2.6) and (2.7) by linear superposition since for linear resistivity J depends linearly on H_a.

Next I discuss some limiting cases where the solutions of (2.16) and (2.17) are known. At low frequencies, $\omega\tau \ll 1$, the induced sheet current (eddy current) is small such that the integrals in (2.16) and (2.17) can be disregarded. One then gets

$$J(y) = 2\pi i\,\omega\tau(\omega)\,y H_0\,, \quad (2.18)$$

$$J(r) = \pi i\,\omega\tau(\omega)\,r H_0\,. \quad (2.19)$$

For Ohmic ρ this means

$$J(y,t) = 2\pi\,y\,\tau\,\dot{H}_a(t)\,, \quad (2.20)$$

$$J(r,t) = \pi\,r\,\tau\,\dot{H}_a(t)\,. \quad (2.21)$$

At high frequencies, $\omega\tau \gg 1$, the term in brackets in (2.16) and (2.17) has to vanish. This is solved by the ideal screening current $J_0(y,t)$ (1.4) or $J_0(r,t)$ (1.5), since one has for $y < 1$ or $r < 1$,

$$\int_0^1 \frac{u}{(1-u^2)^{1/2}}\,S(y,u)\,du = -\pi\,, \quad (2.22)$$

$$\int_0^1 \frac{u}{(1-u^2)^{1/2}}\,P(r,u)\,du = -\frac{\pi^2}{2}\,, \quad (2.23)$$

$$\int_0^1 \frac{u}{(1-u^2)^{1/2}}\, K(y,u)\, du = -\pi y\,, \tag{2.24}$$

$$\int_0^1 \frac{u}{(1-u^2)^{1/2}}\, Q(r,u)\, du = -\frac{\pi^2}{4} r\,. \tag{2.25}$$

The useful relationships (2.22)–(2.25) can be proven by physical arguments (screening of H_a) or by some lengthy calculations. They will be used below to check the accuracy of numerical integration methods.

For purely imaginary $\rho = i\omega\mu_0\lambda^2$, occurring for rigid pinning or in the Meissner state, the frequency drops out from the prefactor $i\omega\tau(\omega) = ad/(2\pi\lambda^2)$, and thus Eqs. (2.16) and (2.17) become time independent integral equations for $J(y)$ and $J(r)$. The time dependence may thus be separated and $H_a(t)$ and $J(y,t)$, $H(y,t)$ or $J(r,t)$, $H(r,t)$ are now *exactly in phase*, in contrast to Eqs. (2.20) and (2.21) and to the skin effect. Two limiting cases may occur:

For $\lambda^2 \ll ad$ the expressions in brackets in (2.16) and (2.17) have to vanish because of the large prefactor $ad/(2\pi\lambda^2)$. The solution is then the ideal screening current (1.4) and (1.5) as discussed above.

For $\lambda^2 \gg ad$ the sheet current becomes so small that the thin film cannot screen the ac field completely. The second term in the brackets in (2.16) and (2.17) may then be dropped, like in the low-frequency limit, and one gets

$$J(y,t) = H_a(t)\, y\, a\, d/\lambda^2, \tag{2.26}$$

$$J(r,t) = H_a(t)\, r a\, d/2\lambda^2\,. \tag{2.27}$$

More general solutions of (2.16) and (2.17) may be obtained by iteration, yielding an expansion in powers of ω (Sec. III), or numerically (Sec. IV).

III. ITERATIVE SOLUTION METHOD

The integral equations (2.16) and (2.17) are formally solved by a power series in ω,

$$J(y) = 2\pi H_0 i\omega\tau\,[\,y + i\omega\tau K y + (i\omega\tau)^2 K^2 y + \cdots\,], \tag{3.1}$$

$$J(r) = \pi H_0 i\omega\tau\,[\,r + i\omega\tau Q r + (i\omega\tau)^2 Q^2 r + \cdots\,], \tag{3.2}$$

with the abbreviations

$$K^n\cdot y = \int_0^1 dy_1 \cdots \int_0^1 dy_n K(y,y_1)\cdots K(y_{n-1},y_n)\, y_n\,, \tag{3.3}$$

$$Q^n\cdot r = \int_0^1 dr_1 \cdots \int_0^1 dr_n Q(r,r_1)\cdots Q(r_{n-1},r_n)\, r_n\,. \tag{3.4}$$

The complex ac magnetic moment $\mathbf{m}$, written as

$$\mathbf{m} = -\hat{\mathbf{x}} M L, \quad M = 2\int_0^a y\, J(y)\, dy \qquad \text{(strip)}, \tag{3.5}$$

$$\mathbf{m} = -\hat{\mathbf{x}} M, \quad M = \pi\int_0^a r^2\, J(r)\, dr \qquad \text{(disk)}, \tag{3.6}$$

formally may be expressed by the series [for brevity I omit the factor $H_0\exp(i\omega t)$]

$$M = 4\pi a^2 i\omega\tau \int_0^1 dy\, y\left[\, y + i\omega\tau\int_0^1 du\, K(y,u)\, u + \cdots\right]$$

$$= 4\pi a^2 \sum_{n=0}^{\infty}\int_0^1 dy\, y\,(K^n y) \qquad \text{(strip)}, \tag{3.7}$$

$$M = \pi^2 a^3 i\omega\tau \int_0^1 dr\, r^2\left[\, r + i\omega\tau\int_0^1 dr\, Q(r,u)\, u + \cdots\right]$$

$$= \pi^2 a^3 \sum_{n=0}^{\infty}\int_0^1 dr\, r^2\,(Q^n r) \qquad \text{(disk)}, \tag{3.8}$$

where $K^0 y = y$, $Q^0 r = r$. This yields

$$M = 4\pi a^2\left[\frac{i\omega\tau}{3} + \frac{\omega^2\tau^2}{2} + \cdots\right] \qquad \text{(strip)}, \tag{3.9}$$

$$M = \pi^2 a^3\left[\frac{i\omega\tau}{4} + \frac{4\omega^2\tau^2}{15} + \cdots\right] \qquad \text{(disk)}. \tag{3.10}$$

Here I have used

$$\int_{-1}^1\int_{-1}^1 y\, u\, \ln|y-u|\, dy\, du = -1\,, \tag{3.11}$$

$$\int_0^1\int_0^1 r^2\, u\, q\left(\frac{r}{u}\right) dy\, du = \frac{4}{15}\,. \tag{3.12}$$

For ideal screening ($\omega\to\infty$) one has $M = M_0$ where $M_0 = \pi a^2$ (strip) and $M_0 = 8a^3/3$ (disk) are obtained by inserting the ideal screening current J_0 (1.4) or (1.5) into M (3.5) or (3.6).

Defining the complex susceptibility by

$$\mu(\omega) = 1 - \frac{M(\omega)}{M_0} = \mu' - i\mu''\,, \tag{3.13}$$

one gets from (3.9) and (3.10) for $\omega\tau \ll 1$

$$\mu' = 1 - 2\omega^2\tau^2, \qquad \mu'' = \frac{4}{3}\omega\tau \qquad \text{(strip)}, \tag{3.14}$$

$$\mu' = 1 - \frac{\pi^2}{10}\omega^2\tau^2, \quad \mu'' = \frac{3\pi^2}{32}\omega\tau \qquad \text{(disk)}. \tag{3.15}$$

The corresponding expressions for $\omega\tau \gg 1$ may be obtained from the short-time behavior of $M(t)$ (Sec. VI) and from the dissipation (1.8) and (1.9), which is related to $\mu''(\omega)$ by

$$P = M_0\,\omega\,\mu''(\omega)\,\mu_0\,\langle H_a(t)^2\rangle\,, \tag{3.16}$$

with $M_0 = \pi a^2$ or $M_0 = 8a^3/3$ from above. This yields for $\omega\tau \gg 1$ (see also Sec. VIII)

$$\mu' = \frac{1}{\pi\omega\tau}, \quad \mu'' = \frac{2}{\pi^2}\frac{\ln(16.2\,\omega\tau)}{\omega\tau} \qquad \text{(strip)}, \tag{3.17}$$

$$\mu' = \frac{3}{2\pi\omega\tau}, \quad \mu'' = \frac{3}{\pi^2}\frac{\ln(11.3\,\omega\tau)}{\omega\tau} \qquad \text{(disk)}. \tag{3.18}$$

From Eqs. (3.14)–(3.18), useful approximate expressions

for the ac susceptibility and ac losses (3.16) in the entire frequency range will be constructed in Sec. VIII, which deviate from the computed results by less than 1% and exhibit the correct asymptotic behavior at low and high frequencies.

IV. NUMERICAL SOLUTION METHOD

The numerical evaluation of the integrals in (2.1), (2.2), (2.6), (2.7), (2.16), and (2.17) requires some care since at large frequencies or short times the sheet current $J(u)$ is sharply peaked near the specimen edges; cf. the ideal screening currents (1.4) and (1.5). Furthermore, the integral kernels $K(y,u)$ (2.9) and $Q(r,u)$ (2.10), and for the disk even the Ampére's-law kernel $P(r,u)$ (2.4), have logarithmic infinities at $y=u$ or $r=u$, as may be seen from the expansions of $p(v)$ (2.14) and $q(v)$ (2.15). For simplicity and for rapid computation, it is desirable to avoid interpolation of $J(u)$ and of the kernels during the integration and iteration but rather use the tabulated values directly. In such computations the searched for function $J(u)$ is a vector $J_i = J(u_i)$ $(i = 1, ..., N)$ and the kernels are matrices, e.g., $Q(r,u) \to Q_{ij} = Q(r_i, r_j)$; the integration then corresponds to a matrix multiplication, e.g., $\int Q(r,u)\,J(u)\,du \to N^{-1}\sum_j Q_{ij}J_j$.

All these requirements are met by the computation method presented in Sec. III B of Ref. 1 for the strip geometry. For the circular disk, this rapid computation method has to be modified in three points.

(a) The kernel $P(r,u)$ (2.4) has now both an odd and an even (logarithmic) infinity at $r/u=1$; cf. the first two terms in the expansion (2.14).

(b) Both kernels $P(r,u)$ and $Q(r,u)$ for the disk are calculated from a tabulated function (Appendix).

(c) The accuracy of the numerical integrals depends on the precision of the constants 4 and 0.079 44 in the expansions (2.14) and (2.15) around $v=1$.

This computation method is based on three ideas.

First idea. The tabulation points $y_i = r_i = u_i$ are taken from a substitution function $y(x) = r(x) = u(x)$ whose derivative $u'(x) = w(x)$ (weight function) vanishes at $u=1$. For convenience we chose $u(0)=0$ and $u(1)=1$ and equidistant points $x_i = (i-\frac{1}{2})/N$ $(i=1,\ldots,N)$, writing $y_i = r_i = u_i = u(x_i)$ and $w_i = u'(x_i)$. Odd functions give better accuracy. Two such functions are

$$u(x) = \frac{3}{2}x - \frac{1}{2}x^3, \qquad w(x) = \frac{3}{2}(1-x^2), \tag{4.1}$$

$$u(x) = \frac{15}{8}x - \frac{5}{4}x^3 + \frac{15}{40}x^5, \quad w(x) = \frac{15}{8}(1-x^2)^2. \tag{4.2}$$

All integrals are then computed as

$$\int_0^1 f(u)\,du = \int_0^1 f[u(x)]\,w(x)\,dx \approx \frac{1}{N}\sum_{i=1}^{N} f(u_i)\,w_i. \tag{4.3}$$

Note that even when the integrand $f(u)$ has an infinity $\sim (1-u)^{-1/2}$ at $u=1$, the new integrand $f[u(x)]\,u'(x)$ does not exhibit an infinity but is constant at $x=1$ or even vanishes as $(1-x)^{1/2}$ when the substitution (4.1) or (4.2) is used, respectively.

The boundary $u=0$ in all our integrals is not a real boundary and does not influence the numerical accuracy because all the integrands in this paper are even, $f(-u) = f(u)$; (4.3) may thus be written as $\frac{1}{2}\int_{-1}^{1} f(u)\,du$. The integration method (4.3) yields thus high accuracy even for small $N = 20, \ldots, 100$.

Second idea. If the integrand $f(u)$ has an infinity $\sim (u-y)^{-1} = (u_j - u_i)^{-1}$, maximum numerical accuracy is achieved by omitting in the sum (4.3) the (infinite) term $j=i$. This is because $(u-y)^{-1}$ is an *odd* function near $u=y$. As opposed to this, a logarithmic infinity $\sim \ln|u-y| = \ln|u_j - u_i|$ is an *even* function. Therefore, omission of the term $j=i$ would yield noticeable inaccuracy. As shown in Ref. 1 [Eq. (3.11)], maximum accuracy is achieved if in the integration sum the term $w_j \ln|u_i - u_j|$ at $j=i$ is replaced by $w_j \ln(w_j/2\pi N)$. Here $w_j/N \approx \frac{1}{2}(u_{j+1} - u_{j-1})$ is the effective distance of the integration points; the constant $\ln(1/2\pi)$ follows from the requirement that the sum exactly equals the integral in the particular case where the integrand is just the logarithm and the integration boundaries are extended to infinity. A possible constant part lnc of the integrand at $u=y$ has to be treated separately. The general replacement prescription for $i=j$ is thus

$$w_j \ln(c|u_i - u_j|) \to w_j \ln(cw_j/2\pi N). \tag{4.4}$$

In particular, with the notation $y \to u_i$, $r \to u_i$, $u \to u_j$ and with the expansions (2.14) and (2.15), the above integral kernels $S(y,u)$, $P(r,u)$, $K(y,u)$, and $Q(r,u)$ in matrix form read

$$S_{i\neq j} = \frac{2u_j w_j}{(u_i^2 - u_j^2)N}, \qquad S_{jj} = 0, \tag{4.5}$$

$$P_{i\neq j} = -\frac{w_j}{u_j N}\,p\left(\frac{u_i}{u_j}\right), \qquad P_{jj} = \frac{w_j}{u_j N}\ln\frac{w_j}{8\pi u_j N}, \tag{4.6}$$

$$K_{i\neq j} = \frac{w_j}{N}\ln\left|\frac{u_i - u_j}{u_i + u_j}\right|, \quad K_{jj} = \frac{w_j}{N}\ln\frac{w_j}{4\pi u_j N}, \tag{4.7}$$

$$Q_{i\neq j} = -\frac{w_j}{N}\,q\left(\frac{u_i}{u_j}\right), \qquad Q_{jj} = \frac{w_j}{N}\ln\frac{0.923\,63 w_j}{2\pi u_j N}. \tag{4.8}$$

The factor $0.923\,63 = \exp(-0.079\,44)$ in (4.8) originates from (2.15). The correct numerical factors in the diagonal terms of (4.6)–(4.8) are important to achieve high accuracy as can be checked by means of the known integrals (2.22)–(2.25). With a wrong choice of constants, the numerical error decreases only slowly as N^{-1} with increasing number N of integration points, while with the correct constants it decreases as N^{-2} or faster. For example, the sums $\sum_{i=1}^{N} f_j K_{ij}$ and $\sum_{i=1}^{N} f_j Q_{ij}$ with $f_j = u_j(1-u_j^2)^{-1/2}$ deviate from their analytical values $-\pi u_i$ (2.34) and $-(\pi^2/4)u_i$ (2.35) by root mean square deviations $\delta = 17\,(4.3)\times 10^{-6}$ or $\delta = 24\,(6.6)\times 10^{-6}$ for $N = 50\,(100)$ with the substitution (4.1). The larger deviation in the disk geometry is due to the fact that the kernel Q_{ij} is interpolated from the tabulated function

$q(v)$ (Appendix).

Interestingly, a very small deviation $\delta = 2 \times 10^{-8}$ (for $N = 100$) is achieved if the substitution function $u(x)$ is chosen as the linear combination 0.835 times $u(x)$ (4.1) plus 0.165 times $u(x)$ (4.2). This observation suggests the interesting mathematical problem to find the optimum substitution function $u(x)$ that minimizes the numerical deviation δ for a given N.

An alternative method to chose the diagonal terms K_{ii} and Q_{ii} is to require that the matrix version of the relation (2.24) or (2.25) hold *exactly*. This condition is satisfied with

$$K_{ii} = -\Big(\pi u_i + \sum_{j\neq i} K_{ij} u_j\Big)/u_i\,, \tag{4.9}$$

$$Q_{ii} = -\Big(\frac{\pi^2}{4} u_i + \sum_{j\neq i} Q_{ij} u_j\Big)/u_i\,. \tag{4.10}$$

This choice yields similar accuracy as (4.7) or (4.8).

The basic equations (2.1), (2.2), (2.6), and (2.7) in matrix form explicitly read [writing $H(y_i) = H(r_i) = H_i$ and $J(y_i) = J(r_i) = J_i$]

$$H_i = H_a + \frac{1}{2\pi}\sum_{j=1}^{N} S_{ij} J_j\,, \tag{4.11}$$

$$H_i = H_a + \frac{1}{2\pi}\sum_{j=1}^{N} P_{ij} J_j\,, \tag{4.12}$$

$$J_i(t) = 2\pi\,\tau\,\dot H_a(t) + \tau\sum_{j=1}^{N} K_{ij}\dot J_j(t)\,, \tag{4.13}$$

$$J_i(t) = \pi\,\tau\,\dot H_a(t) + \tau\sum_{j=1}^{N} Q_{ij}\dot J_j(t)\,. \tag{4.14}$$

Third idea. In the equations of motion for $J(y,t)$ (2.16) and $J(r,t)$ (2.17) the time derivative $\dot J$ is on the "wrong" side such that a direct numerical time integration is not possible. However, in the matrix forms (4.13) or (4.14) the time integration poses no problem since these equations may be solved for the vector $\dot J_i(t)$ by just inverting the matrix $K_{ij} \to K_{ij}^{-1}$ or $Q_{ij} \to Q_{ij}^{-1}$. The resulting linear differential equations

$$\dot J_i(t) = \sum_{j=1}^{N} K_{ij}^{-1}[\,J_j(t)/\tau - 2\pi\,H_a(t)\,u_j\,]\,, \tag{4.15}$$

$$\dot J_i(t) = \sum_{j=1}^{N} Q_{ij}^{-1}[\,J_j(t)/\tau - \pi\,H_a(t)\,u_j\,] \tag{4.16}$$

are easily integrated by a Runge-Kutta method starting with the known vector $J_i(0)$ at $t = 0$; see Sec. V for an example. This numerical integration is stable if the time step dt is sufficiently small, $dt \le 5/N^2$ or $dt \le 10/N^3$ if the substitution (4.1) or (4.2) is chosen, respectively, or $dt \le 2/N$ if $u = x$ is not substituted. For general substitution one should try $dt \le 10(1 - y_N)$ where y_N is the tabulated point closest to the specimen edge.

Note that in (4.15) and (4.16) the relaxation time $\tau(T, B, J)$ in general may depend on position and time implicitly via its dependence on B and J meaning that $\tau = \tau_j(t)$. In a homogeneous material with linear resistivity, τ is constant.

To conclude this section I give here also the matrix form of Eqs. (2.16) and (2.17) in frequency space, which will be required in Sec. VII,

$$J_i = i\omega\tau(\omega)\left[\,2\pi H_0 u_i + \sum_{j=1}^{N} K_{ij}\,J_j\,\right], \tag{4.17}$$

$$J_i = i\omega\tau(\omega)\left[\,\pi H_0 u_i + \sum_{j=1}^{N} Q_{ij}\,J_j\,\right]. \tag{4.18}$$

V. PENETRATION OF A FIELD JUMP

In this section I consider the example of an Ohmic disk to which a suddenly switched on field $H_a(t) = \Theta(t)$ is applied [$\Theta(t < 0) = 0$, $\Theta(t \ge 0) = 1$]. The corresponding problem for the strip is treated in Sec. IV of Ref. 1. The sheet current $J(r,t)$ induced in the disk by this field jump and decaying due to Ohmic dissipation follows from Eqs. (1.5) and (2.7). Choosing the disk radius a as unit length, one has to solve the equations

$$\begin{aligned} &J(r,t) = 0 && \text{for } t < 0\,,\\ &J(r,t) = (4r/\pi)(1-r^2)^{-1/2} && \text{for } t = 0\,,\\ &J(r,t) = \tau\int_0^1 \dot J(u,t)\,Q(r,u)\,du && \text{for } t \ge 0\,, \end{aligned} \tag{5.1}$$

with $Q(r,u)$ from (2.10). At large times $t \gg \tau$ the circulating current decreases exponentially as

$$J(r, t \gg \tau) = c_J f_0(r)\exp(-t/\tau_0)\,, \tag{5.2}$$

where $c_J = 1.663$ is obtained by numerical integration of (5.1). As with the strip, the function $f_0(r)$ here is normalized to $\int_0^1 f_0(r)^2\,dr = 1$. The relaxation time $\tau_0 = \tau/\Lambda_0$ follows from the lowest eigenvalue Λ_0 of the eigenvalue problem obtained by inserting (5.2) into (5.1),

$$f_n(r) = -\Lambda_n\int_0^1 f_n(u)\,Q(u,r)\,du\,. \tag{5.3}$$

Solving (5.3) iteratively by the matrix method of Sec. IV, we get $\Lambda_0 = 0.876\,867\ldots$. The fundamental relaxation time of an Ohmic disk is thus

$$\tau_0 = \tau/\Lambda_0 = 0.181\,50\,a d\mu_0/\rho\,. \tag{5.4}$$

This relaxation time is smaller than the relaxation time of an Ohmic strip $\tau_0 = 0.249\,24\,a d\mu_0/\rho$ (Ref. 1) by a factor $0.638\,57/0.876\,87 = 0.728$. As with the strip, the higher eigenvalues are $\Lambda_n \approx \Lambda_0 + n$ for all $n = 0, 1, 2, 3, \ldots$.

The lowest eigenfunction (fundamental mode) $f_0(r)$ is shown in Fig. 5 together with the corresponding field profile. The slope f_0' is $f_0'(0) = 3.120$ at the disk center and diverges logarithmically at the disk edge; this is

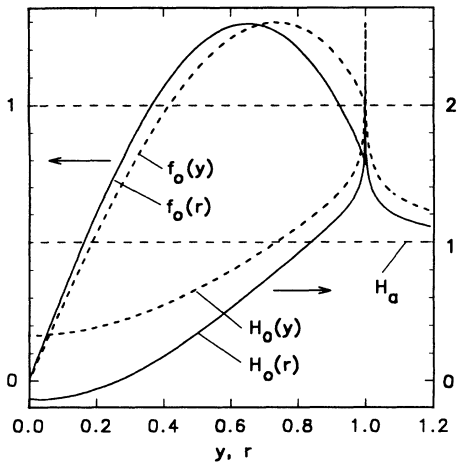

FIG. 5. The lowest eigenfunctions $f_0(y)$ [dashed line, Eq. (4.5) of Ref. 1] and $f_0(r)$ [solid line, Eq. (5.3)], which describe the profile of the sheet current in an Ohmic strip or disk long time after a change of the applied magnetic field (fundamental relaxation modes). Also shown are the corresponding magnetic field profiles $H_0(y)$ (dashed lines) and $H_0(r)$ (solid lines) obtained by inserting the sheet current $f_0(y)$ into (2.1) or $f_0(r)$ into (2.2) and putting $H_a = 1$. The amplitudes of f_0 and H_0 have no physical meaning since f_0 is normalized.

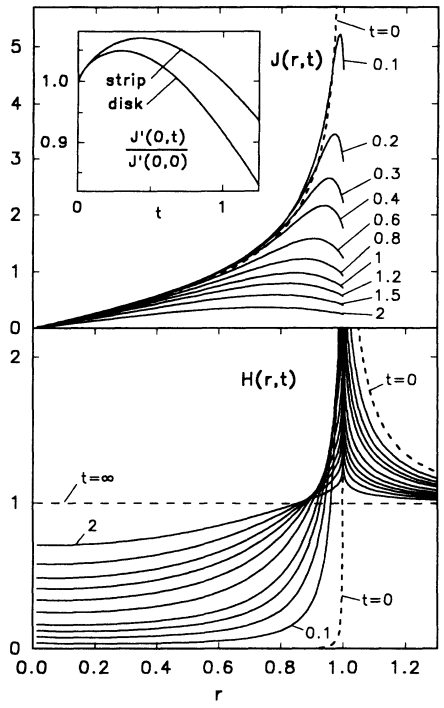

FIG. 6. Decaying sheet current $J(r,t)$ and the penetrating magnetic field $H(r,t)$ in an Ohmic disk after a sudden jump of the applied perpendicular field $H_a(t) = \Theta(t)$. Parameter is the time $t = 0$, 0.1, 0.2, 0.3, 0.4, 0.6, 0.8, 1, 1.2, 1.5, 2 in units of $\tau = ad/2\pi D$, $D = \rho/\mu_0$. The inset shows the time dependence of the slopes $J'(y,t)$ and $J'(r,t)$ of the current profiles in the center of the strip ($y = 0$) or disk ($r = 0$). The slopes have a maximum at $t = 0.43$ or $t = 0.30$, respectively.

evident from Eq. (5.3) since the kernel (2.10) has a logarithmic infinity (2.15). One has $f_0(1) = 0.7839$ and a maximum $f_{0\max} = 1.2929$ at $r = 0.650$. For the magnetization we shall need below $\int_0^1 f_0(r)\, r^2\, dr = c_f = 0.3704$. The fundamental modes $f_0(y)$ and $f_0(r)$ for the strip and disk are approximated with root mean square deviation $\delta = 0.0019$ (for both strip and disk) by the polynomials

$$f_0(y) \approx 2.7267y - 2.0156y^3 + 0.6137y^5 - 0.3132y^7 , \tag{5.5}$$

$$f_0(r) \approx 3.1239r - 3.1045\, r^3 + 1.1631r^5 - 0.3867r^7 . \tag{5.6}$$

Remarkably, with the appropriate normalization for the disk $\int_0^1 f_n(r)^2 r\, dr = 1$ one has the boundary value $f_n(1) = 1$ (for $n \ll N$, like with the strip) and the orthogonality $\int_0^1 f_m(r) f_n(r) r\, dr = \delta_{mn}$ as opposed to $\int_0^1 f_m(r) f_n(r)\, dr = \delta_{mn}$ for the strip.

The sheet current $J(r,t)$ induced in the disk by a sudden field change of unit amplitude and the local perpendicular field $H(r,t)$, obtained by integrating Eqs. (5.1) and (2.1) by the matrix method of Sec. IV, are shown in Fig. 6. As for the strip, at finite times $t > 0$ the $(1-r^2)^{-1/2}$ infinities of $J(r,t)$ and $H(r,t)$ at the edges are removed: The infinity of $J(r,t)$ gets rounded such that initially the peak moves away from the edge with constant velocity $v = 0.77\rho/(\mu_0 d)$. This velocity depends only on the thickness d of the conductor but not on its form (strip, disk, rectangle, etc.). In $H(r,t)$, a weak logarithmic infinity at the edges occurs at all times. Clearly, all these infinities are smeared when the finite specimen thickness d is accounted for.

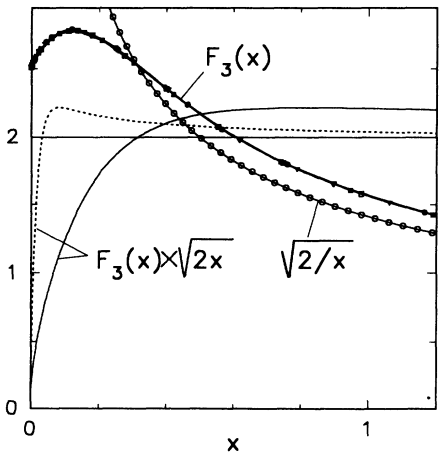

FIG. 7. Self-similarity of the sheet current near the edge of an Ohmic strip or disk, and of thin conductors of any shape, at short times after a jump of the applied perpendicular magnetic field. By scaling the sheet current according to (5.7), (5.8) the current profiles for times $10^4 \times t = 4$, 10, 21, 33, 47, and 62 (solid lines with different symbols) collapse into one curve $F_3(x)$; see also Fig. 15. The curve $(2/x)^{1/2}$ indicates the ideal screening current. Also shown is the function $F_3(x)(2x)^{1/2}$ (solid line) and the same curve compressed along x by a factor of 10.

The sheet current at short times $t \ll \tau$ exhibits scaling behavior, like with the strip [Eq. (7.3) of Ref. 1],

$$J(y,t) = \left(\frac{\tau}{t}\right)^{1/2} F_3\left(\frac{a-|y|}{a}\,\frac{\tau}{t}\right), \tag{5.7}$$

$$J(r,t) = \left(\frac{\tau}{t}\right)^{1/2} \frac{2}{\pi} F_3\left(\frac{a-r}{a}\,\frac{\tau}{t}\right). \tag{5.8}$$

Here $F_3(x)$ is a universal function shown in Fig. 7, with $F_3(0) \approx 2.51$, a maximum $F_{3\max} \approx 2.787$ at $x_{\max} \approx 0.123$, and with $F_3(x) \approx (2/x)^{1/2}$ for $x \gg 1$. The function $F_3(x)(x/2)^{1/2}$ has a maximum value 1.11 at $x = 0.82$ and approaches unity for $x \gg 1$. The factor $2/\pi$ in (5.8) originates from the different amplitudes of the ideal screening currents (1.4) and (1.5).

The slope $J'(0,t)$ of the sheet current at the center of the strip or disk (inset in Fig. 6) initially takes the value 2 $(4/\pi)$, then *increases* as the sheet current penetrates, and reaches a maximum value 1.070×2 $(1.049 \times 4/\pi)$ at $t/\tau = 0.43$ (0.30); at $t \gg \tau$ this slope relaxes as $J'(0,t) = 5.94$ (5.18) $\exp(-t/\tau_0)$ with the τ_0 for the strip or disk.

VI. MAGNETIZATION AFTER A FIELD JUMP

The relaxing negative magnetic moment of the Ohmic disk $M(t)$ (3.6) calculated from the sheet current $J(r,t)$ is shown in Fig. 8. At $t = 0$ one has ideal diamagnetic screening with $M(t=0) = M(\omega \to 0) = M_0 = (8/3)a^3 H_a$ (or $M_0 = 8/3$ in reduced units). At short times $t \ll \tau$, $M(t)$ has a logarithmic cusp, like with the strip,

$$M(t)/M_0 \approx 1 + c_1 t \ln(t/c_2\tau), \tag{6.1}$$

$$\dot{M}(t)/M_0 \approx c_1(1 - \ln c_2) + c_1 \ln(t/\tau). \tag{6.2}$$

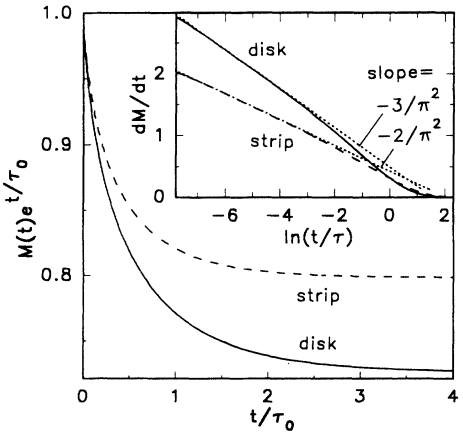

FIG. 8. Magnetization $M(t)$ (3.5), (3.6) of an Ohmic strip (dashed line) and disk (solid line) after a sudden jump of the applied perpendicular field. Shown is $M(t)\exp(t/\tau_0)$ as a function of t/τ_0 where τ_0 is the relaxation time of the strip ($\tau_0 = 0.2492ad/D$) or disk ($\tau_0 = 0.1815ad/D$) (5.4). The inset shows the time derivative dM/dt as a function of the natural logarithm of t/τ where $\tau = ad/2\pi D$. For short times these curves are straight lines (6.2) of slope $-2/\pi^2$ (strip) and $-3/\pi^2$ (disk) as indicated by the dotted lines.

This cusp originates from the higher eigenmodes $f_n(r)$ of (5.3). One has the exact values $c_1 = 2/\pi^2$ for the strip and $c_1 = 3/\pi^2$ for the disk; cf. Eqs. (3.17) and (3.18) and Sec. VIII below. Numerical fits to Eq. (6.2) yield $c_2 = 25.0$ for the strip and $c_2 = 17.7$ for the disk. The logarithmic time dependence of $\dot{M}(t)$ (6.2) leads to the $1/\omega$ behavior of the complex susceptibility $\mu(\omega)$ (3.17) and (3.18) at large frequencies. The more pronounced square root cusp $M(t) - 1 \sim \sqrt{t}$ in the longitudinal geometry leads to $\mu(\omega) \sim (1-i)/\sqrt{\omega}$ which is typical for diffusive behavior and will be discussed below.

At large times $t \gg \tau_0$, one has

$$M(t)/M_0 = c_M \exp(-t/\tau_0), \tag{6.3}$$

with $c_M = 2c_f c_J/\pi = 0.7982$, $\tau_0 = 0.249ad/D$ for the strip and $c_M = \pi c_f c_J \frac{3}{8} = 0.7255$, $\tau_0 = 0.182ad/D$ for the disk. Both c_M values are close to the corresponding prefactors in parallel geometry, namely, $c_M = 8/\pi^2 = 0.811$ for slabs, $c_M = 0.692$ for cylinders, and $c_M = 64/\pi^4 = 0.657$ for bars with square cross section; see below.

For comparison I give here first the penetrating magnetic field $H(x,t)$ and $H(r,t)$ and the relaxing negative magnetic moment (or averaged magnetization) $M(t)$ for a slab of thickness d and a cylinder of radius R in longitudinal field $H_a(t) = \Theta(t)$. The current density in these cases is simply $j(x,t) = H'(x,t)$ and $j(r,t) = H'(r,t)$. One has for the slab (cf. Sec. II of Ref. 1),

$$H(x,t) = 1 - \frac{4}{\pi}\sum_{n=0}^{\infty} \frac{\cos[\frac{\pi x}{d}(2n+1)]}{(-1)^n(2n+1)} e^{-t/\tau_n}, \tag{6.4}$$

$$M(t) = \frac{8}{\pi^2}\sum_{n=0}^{\infty} (2n+1)^{-2} e^{-t/\tau_n}, \tag{6.5}$$

with $\tau_n = \tau_0/(2n+1)^2$, $\tau_0 = d^2/(\pi^2 D)$, $D = \rho/\mu_0$ (diffusivity of flux and current).

For the cylinder a similar expansion of $H(r,t)$ in terms of Bessel functions $J_0(x)$ yields

$$H(r,t) = 1 - \sum_{n=0}^{\infty} \frac{2\,J_0(k_n r)}{x_n J_1(x_n)} e^{-t/\tau_n}, \tag{6.6}$$

$$M(t) = 4\sum_{n=0}^{\infty} x_n^{-2} e^{-t/\tau_n}, \tag{6.7}$$

where $\tau_n = 1/(k_n^2 D) = R^2/(x_n^2 D)$, $k_n = x_n/R$, and x_n are the zeros of $J_0(x)$, e.g., $x_0 = 2.4048$, $x_1 = 5.5201$, $x_n \approx \pi(n+\frac{3}{4}) + 1/[8\pi(n+\frac{3}{4})]$. Thus, $\tau_0 = R^2/(x_0^2 D) = R^2/(5.783D)$. In particular, at $t = 0$ one has $H(r,0) = 0$ for $r \le R$ (ideal screening) and $M(t) = 1$ since $\sum x_n^{-2} = 1/4$. At short times $t \ll \tau_0$ one gets in this longitudinal geometry for slabs and cylinders,

$$1 - M(t) \approx \frac{4}{d}(tD/\pi)^{1/2} = 4\pi^{-3/2}(t/\tau_0)^{1/2}, \tag{6.8}$$

$$1 - M(t) \approx \frac{4}{R}(tD/\pi)^{1/2} = \frac{4\pi^{-1/2}}{5.783}(t/\tau_0)^{1/2}. \tag{6.9}$$

The cusps (6.8) and (6.9) may be derived noting that at short times the surface shielding current $j(\xi,t) = (\pi Dt)^{-1/2}\exp(-\xi^2/4Dt)$ ($\xi = d/2 - |x|$ or $\xi = R - r$) diffuses away from the surface and flows at an average depth $\langle\xi\rangle = (4Dt/\pi)^{1/2}$ in slabs and cylinders. Note, however, the different definitions of M for cylinders (or disks) and slabs (or strips); cf. Eqs. (3.3) and (3.4). The current along a large flat surface (or edge) counts twice since it has to perform a U turn at the two faraway ends which gives the same contribution to the magnetic moment as the surface current. For the slab the diffusion reduces both contributions equally: During diffusion, the current along the flat surface keeps its size, $\int_0^{d/2} j(x,t)\,dx = H_a = 1$ for $t \ll \tau_0$, but flows closer to the central plane of the slab; in contrast to this, the U-turn current keeps its (large) distance from the center of the slab but its path length is reduced. Both reductions of M have to be equal because of $\mathrm{div}\mathbf{j} = 0$.

At large times $t \gg \tau_0$, (6.6) and (6.7) yield $M(t) = c_M \exp(-t/\tau_0)$ with $c_M = 8/\pi^2 = 0.811$ (slab) and $c_M = 4/2.405^2 = 0.691\,66$ (cylinder) as stated above.

Finally I give here also the results for an Ohmic slab or bar with rectangular cross section $d \times b$ filling the space $0 \le x \le d$, $0 \le y \le b$, $-\infty \le z \le \infty$. In a jumping longitudinal field $H_a(t) = \Theta(t)$, the penetrating field $H(x,y,t)$ and the negative magnetic moment per unit volume $M(t) = 1 - \langle H(x,y,t)\rangle_{x,y}$ are derived straightforwardly from the diffusion equation $\dot{H} = D\nabla^2 H$ with $D = \rho/\mu_0$. This yields

$$H(x,y,t) = 1 - \frac{16}{\pi^2}\sum_\mu\sum_\nu \frac{\sin\frac{\pi x\mu}{d}\sin\frac{\pi y\nu}{b}}{\mu\,\nu} e^{-\frac{t}{\tau_{\mu\nu}}}, \quad (6.10)$$

$$M(t) = \frac{64}{\pi^4}\sum_\mu\sum_\nu \frac{e^{-\frac{t}{\tau_{\mu\nu}}}}{\mu^2\,\nu^2}, \quad (6.11)$$

$$\tau_{\mu\nu}^{-1} = D\pi^2(\mu^2/d^2 + \nu^2/b^2). \quad (6.12)$$

The sums are over all positive odd integers $\mu,\nu = 1,3,5,\ldots$. The relaxation time of the fundamental mode $\mu = \nu = 1$ is

$$\tau_0 = 1/[D\pi^2(d^{-2} + b^{-2})]. \quad (6.13)$$

For $b \gg d$, Eqs. (6.10) and (6.11) reproduce the results (6.4) and (6.5) for the infinite slab, and for $d = b$ they describe the field penetration into a bar with square cross section. The magnetization of the square rod (6.10) and of the long cylinder (6.7) are quite similar; cf. Fig. 8. The relaxation time $\tau_0 = d^2/(2\pi^2 D)$ of the square bar and $\tau_0 = R^2/(5.783\,D)$ of the cylinder coincide if $R = 0.54d$ or $\pi R^2 = 0.92d^2$.

The magnetization of a rectangular bar exhibits an interesting relaxation law at large times. Note that $M(t) = M_{\mathrm{rect}}(t)$ (6.11) may be written as a product of two factors $M_{\mathrm{slab}}(t)$ (6.5) describing the penetration of flux along x and y, or into slabs of width d and b,

$$M_{\mathrm{rect}}(t) = M_{\mathrm{slab}}(t) \times M_{\mathrm{slab}}(t\,d^2/b^2). \quad (6.14)$$

This means that with increasing aspect ratio b/d the limit of a slab with thickness d is reached very slowly since the second factor in (6.14) is not exactly unity but varies considerably due to its square root cusp (6.8) at $t = 0$. As a consequence, at large but still finite ratio $b/d \gg 1$, the relaxation of M in principle occurs in two steps, the prefactor being first $c_{M,\,\mathrm{slab}} = 8/\pi^2$, and then slowly changing to $c_{M,\,\mathrm{square}} = (8/\pi^2)^2$. At short times one has

$$1 - M(t) \approx 4\frac{d+b}{db}\left(\frac{tD}{\pi}\right)^{1/2} = \frac{4}{\pi^{3/2}}\frac{d+b}{(d^2+b^2)^{1/2}}\left(\frac{t}{\tau_0}\right)^{1/2}. \quad (6.15)$$

For long bars with arbitrary cross section one finds from a skin-depth argument immediately after a longitudinal field jump,

$$M(t) \approx 1 - \frac{\text{surface}}{\text{volume}}\,2\left(\frac{tD}{\pi}\right)^{1/2}. \quad (6.16)$$

VII. ac CURRENT AND FIELD

When a transverse ac field $H_a(t) = \exp(i\omega t)$ is applied to the strip or disk, the complex sheet current $J(y,\omega)$ or $J(r,\omega)$ can be calculated by iterating the integral equation (2.16) or (2.17) or their matrix version (4.17) or (4.18), starting with $J = 0$. This numerical procedure is equivalent to the summation of the power series (3.1) or (3.2) in ω. It converges rapidly for $\omega\tau \le 2\pi$ if a convergence factor $c < 1$ is introduced by iterating not the original equation $J = F\{J\}$ but a modified equation $J = (1-c)J + cF\{J\}$. A small value $c \ll 1$ has to be used when the integration points y_i or r_i are closely spaced, i.e., when N is large or the substitution (4.2) is used.

At larger frequencies $\omega\tau \ge 2\pi$ a faster convergence is achieved if one iterates the inverted equation. This means, instead of solving the matrix equation (4.17) or (4.18) for the vector J_i, one inverts the integral kernel K or Q as required also in Eq. (4.15) or (4.16), and then iterates the equivalent equations

$$J_i = \sum_{j=1}^{N} K_{ij}^{-1}\left[\frac{1}{i\omega\tau}J_j(\omega) - 2\pi\,u_j\right], \quad (7.1)$$

$$J_i = \sum_{j=1}^{N} Q_{ij}^{-1}\left[\frac{1}{i\omega\tau}J_j(\omega) - \pi\,u_j\right], \quad (7.2)$$

starting with the ideal screening solution $J_0(y,t)$ (1.4) or $J_0(r,t)$ (1.5). In the range $3 \le \omega\tau \le 10$ where both methods converge well, the obtained solutions are identical as it should be. Alternatively, the $J_i(\omega)$ may also be calculated by direct inversion of a matrix from (7.1) and (7.2), or as a sum over the eigenfunctions of Eq. (5.3) with frequency dependent amplitudes. The latter method will be used in a projected paper on the linear ac response for complex resistivity.

The ac sheet current $J(r,\omega) = J' + iJ''$ in the disk obtained by this iteration and the corresponding perpendicular field $H(r,\omega) = H' + iH''$ are shown in Figs. 9 and 10. Here J' and H' are the in-phase components, and J'' and H'' are out of phase by $\pi/2$ with respect to the applied field $H_a(t) = \exp(i\omega t)$. One can see that the

current and field profiles for the disk look very similar to those for the strip (Figs. 9 and 10 of Ref. 1). The real part $J'(y,\omega)$ looks similar as $J(y,t)$ in Fig. 6, but $H'(y,\omega)$ penetrates more slowly than $H(y,t)$ in Fig. 6. The imaginary parts $J''(y,\omega)$ and $H''(y,\omega)$ depend nonmonotonically on ω as does the dissipative part μ'' of the ac susceptibility.

Close to the specimen edge the sheet currents of the strip and disk at large frequencies scale as

$$J(y,\omega) = (\omega\tau)^{1/2} F_4\Big(\frac{a-|y|}{a}\,\omega\tau\Big)\,, \tag{7.3}$$

$$J(r,\omega) = (\omega\tau)^{1/2}\frac{2}{\pi} F_4\Big(\frac{a-r}{a}\,\omega\tau\Big)\,, \tag{7.4}$$

where $F_4(x)$ is a universal complex function shown in the inset in Fig. 9; cf. also Eqs. (5.7) and (5.8), and Eq. (7.4) of Ref. 1. This means that, at sufficiently large frequencies of the perpendicular ac field, the complex sheet current near the edges of a flat Ohmic conductors of arbitrary shape and constant thickness d has a *universal profile* $\sim F_4(x)$ with x = distance from the edge times frequency times $d\mu_0/\rho$ times a shape dependent constant which equals $1/(2\pi)$ for both the strip and the circular disk. The amplitude of this universal current profile is $\sim \omega^{1/2}$. The factor $2/\pi$ in (7.4) is the ratio of the ideal shielding currents (1.4) and (1.5). From the general relation

$$J(y,\omega) = i\,\omega\int_0^\infty J(y,t)\,e^{-i\omega t}\,dt\,, \tag{7.5}$$

where $J(y,t)$, or $J(r,t)$, is the sheet current induced by a field jump (cf. Sec. V), one obtains a relationship between the profiles $F_3(x)$ [(5.7) and (5.8)] and $F_4(x)$ [(7.3) and (7.4)],

$$F_4(x) = i\int_0^\infty F_3\Big(\frac{x}{u}\Big)\,u^{-1/2}\,e^{-iu}\,du\,. \tag{7.6}$$

In particular, one has at the very edge ($x = 0$)

$$F_4(0) = (\pi i)^{1/2}F_3(0) = (1+i)(\pi/2)^{1/2}F_3(0)\,, \tag{7.7}$$

$$J(0,\omega) = (1+i)(\pi\omega t/2)^{1/2}\,J(0,t)\,. \tag{7.8}$$

This means the real and imaginary parts of $J(y,\omega)$ or of $J(r,\omega)$ at the specimen edge are equal: The complex

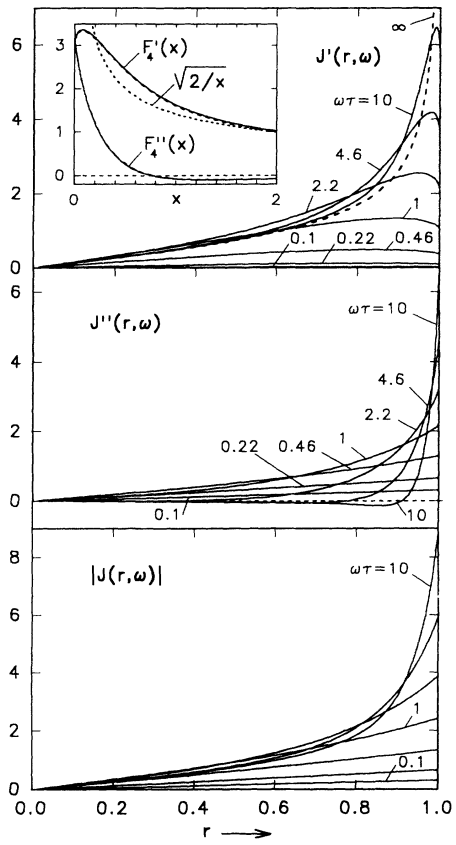

FIG. 9. Complex ac sheet current $J(r,\omega) = J' + iJ''$ in an Ohmic disk in perpendicular ac field of unit amplitude, the solution of the integral equation (2.17) or of the matrix equation (4.16) or (7.2). Depicted are the real and imaginary parts and the modulus of J for $\omega\tau = 0.1$, 0.22, 0.46, 1, 2.2, 4.6, and 10. The dashed curve gives the ideal screening current occurring for $\omega = \infty$. The inset shows the scaling (self-similarity) of the sheet current near the edge of the disk at large frequencies. The plotted curves for $\omega\tau = 46.4$ (solid lines) and $\omega\tau = 21.5$ (dashed lines) nearly coincide into one universal scaling function $F_4(x) = F_4' + iF_4''$ defined by (7.3). (7.4); see also Fig. 15.

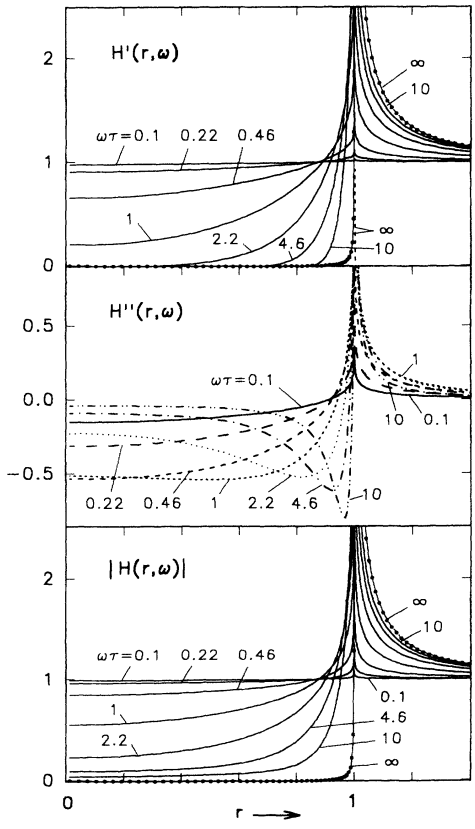

FIG. 10. Complex ac magnetic field $H(r,\omega) = H' + iH''$ in an Ohmic disk in perpendicular ac field of unit amplitude. Depicted are the real and imaginary parts and the modulus of the field obtained by inserting the sheet current $J(r,\omega)$ of Fig. 9 into (2.2) for $\omega\tau = 0.1$, 0.22, 0.46, 1, 2.2, 4.6, and 10.

current density has a phase shift of $\pi/4$ not only at the surface of Ohmic conductors in *longitudinal* ac field (the well known skin effect), but also at the edge of flat conductors in *perpendicular* ac field.

The universal function $F_4(x) = F_4' + iF_4''$ obtained numerically is shown in the inset of Fig. 9 for $\omega\tau = 21.5$ and $\omega\tau = 46.4$; due to the scaling property, both curves coincide within line thickness. One has $F_4(0) = 3.15(1+i)$; $F_4'(x)$ has a maximum value 3.363 at $x \approx 0.074$ and approaches $(2/x)^{1/2}$ for $x \gg 1$; $F_4''(x)$ changes sign at $x = 0.80$ and approaches zero from below for $x \gg 1$.

VIII. COMPLEX ac SUSCEPTIBILITY

The ac susceptibility $\mu(\omega) = \mu' - i\mu''$ (3.13) is calculated as follows. The complex magnetic moment $M(\omega)$ (1.3) of the disk may be obtained by integrating $\pi r^2 J(r,\omega)$ (3.6) over r for many ω values. However, for nondispersive ρ a much faster method exits. One may calculate $\mu(\omega)$ from the real magnetization $M(t)$ of Sec. VI using the relation

$$M(\omega) = i\omega \int_0^\infty M(t)\, \exp(-i\omega t)\, dt\,, \tag{8.1}$$

which with $\mu(\omega) = 1 - M(\omega)/M_0$ (3.13) yields

$$\mu(\omega) = -\frac{1}{M_0}\int_0^\infty \dot{M}(t)\, \exp(-i\omega t)\, dt\,. \tag{8.2}$$

The resulting susceptibility $\mu(\omega) = \mu' - i\mu''$ is shown in Fig. 11; μ'' has a maximum $\mu''_{\max} = 0.4411$ at $\omega_{\max} = 1.025/\tau = 1.169/\tau_0 = 6.440\rho/(\mu_0 ad)$.

The limiting expressions of $\mu(\omega)$ for small and large ω are given for the disk by Eqs. (3.15) and (3.18). From these asymptotes I construct useful analytic expressions which have the correct asymptotic behavior and fit the

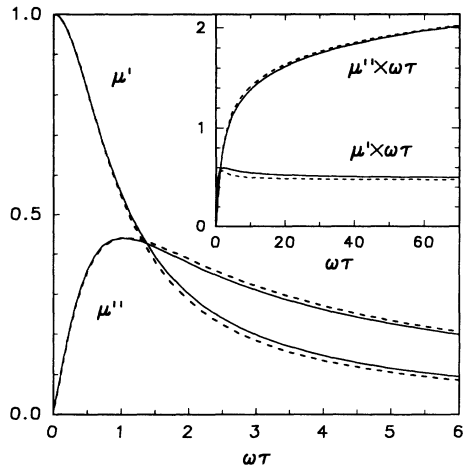

FIG. 11. The ac susceptibility $\mu(\omega) = \mu' - i\mu''$ for the Ohmic circular disk plotted versus $\omega\tau$ with $\tau = ad/2\pi D$, $D = \rho/\mu_0$. Also shown are the approximate expressions (8.3) and (8.4) (dashed lines). The inset shows $\mu'\omega\tau$ and $\mu''\omega\tau$ (solid lines) together with the approximations (8.3) and (8.4) up to large frequencies. Note the excellent fit.

functions $\mu'(\omega)$ and $\mu''(\omega)$ of the disk in perpendicular geometry in the entire frequency range $-\infty < \omega < \infty$ (cf. the dashed lines in Fig. 11),

$$\mu'(\omega) \approx \left[1 - c + \left(c^2 + \frac{4\pi^2}{9}\omega^2\tau^2\right)^{1/2}\right]^{-1}, \quad c = \frac{20}{9}\,, \tag{8.3}$$

$$\mu''(\omega) \approx \left[\frac{32}{3\pi^2 x} + \frac{2\pi^2 x/3}{\ln(x^2+1) + 4.85}\right]^{-1}, \quad x = \omega\tau\,. \tag{8.4}$$

The constant $c = 20/9 = 2.22$ in (8.3) is related to the integral (3.12) which determines the curvature of $\mu'(\omega)$ (3.15). The simple expressions (8.3) and (8.4) deviate from the exact μ' by $< 1.6 \times 10^{-2}$ and from μ'' by $< 1.1 \times 10^{-2}$ only. They do not contain any fitting parameter apart from the constant $4.85 = 2\ln 11.3$ which was adjusted at $\omega \to \infty$.

For comparison I give here also the complex susceptibilities for the strip in perpendicular field and for the slab, cylinder, and rectangular bar in longitudinal field. For the Ohmic strip a similar (and even more accurate) approximate expression for $\mu(\omega) = \mu' - i\mu''$ was constructed from its asymptotic behavior in Ref. 1,

$$\mu'(\omega) \approx [1 - c + (c^2 + \pi^2\omega^2\tau^2)^{1/2}]^{-1}, \quad c = \pi^2/4\,, \tag{8.5}$$

$$\mu''(\omega) \approx \left[\frac{3}{4x} + \frac{\pi^2 x}{\ln(x^2+1) + 5.57}\right]^{-1}, \quad x = \omega\tau\,. \tag{8.6}$$

The success of the interpolation formulas (8.3) and (8.4) suggests the following construction of approximate susceptibilities $\mu(\omega) = \mu' - i\mu''$ from the limiting expressions for high and low frequencies, $\mu''_{\rm low}(\omega)$ and $\mu''_{\rm high}(\omega)$: namely,

$$\mu''(\omega) \approx \left[\frac{1}{\mu''_{\rm low}(\omega)} + \frac{1}{\mu''_{\rm high}(\omega)}\right]^{-1}. \tag{8.7}$$

The real part $\mu'(\omega)$ may then be obtained from the Kramers-Kronig dispersion relation

$$\mu'(\omega) = \frac{2}{\pi}\int_0^\infty \frac{x\,\mu''(x)}{x^2 - \omega^2}\, dx\,. \tag{8.8}$$

If the condition $\mu'(0) = 1$ holds, it may be used to improve this approximation further.

The expression (8.7) is exact for the Debye law $\mu(\omega) = (1 + i\omega\tau)^{-1}$ and is an excellent approximation in perpendicular geometry. In longitudinal geometry such fits are not needed since exact solutions are available for the general rectangular cross section and for the cylinder. Fourier transforming the various expressions for $M(t)$ in Sec. VI according to (8.2) and noting that $M_0 = 1$ in longitudinal geometry, one obtains the following complex susceptibilities in longitudinal ac field.

For a slab of thickness d one gets from (6.4) and (6.5),

$$H(x,\omega)= \cosh(x/\lambda_{ac})/\cosh(d/2\lambda_{ac})\,, \tag{8.9}$$

$$\mu(\omega)= \frac{\langle H(x,\omega)\rangle}{H_a} = \frac{\tanh u}{u} = \frac{(\sinh v+\sin v)-i(\sinh v-\sin v)}{v(\cosh v+\cos v)}\,, \tag{8.10}$$

with $\lambda_{ac} = (1-i)\delta/2$, $u = d/2\lambda_{ac}$, and $v = (1-i)u = (\omega d^2\mu_0/2\rho)^{1/2}$ where $\delta = (2\rho/\mu_0\omega)^{1/2}$ is the skin depth, or $v = (\omega\tau_0\pi^2/2)^{1/2} = d/\delta$ where $\tau_0 = d^2/(\pi^2 D)$ is the relaxation time of the fundamental mode of the slab. The average $\langle H(x,t)\rangle$ is taken over the specimen volume.

For a cylinder of radius R one has from (6.6) and (6.7),

$$H(r,\omega) = I_0(r/\lambda_{ac})/I_0(R/\lambda_{ac})\,, \tag{8.11}$$

$$\mu(\omega) = \frac{\langle H(r,\omega)\rangle}{H_a} = \frac{2\,I_1(u)}{u\,I_0(u)}\,, \tag{8.12}$$

where $u = R/\lambda_{ac} = (1+i)R/\delta$ and $I_0(x)$ and $I_1(x) = I_0'(x)$ are modified Bessel functions. This yields for $\omega\tau_0 \ll 1$, $\mu' = 1 - 0.609\,65\,\omega^2\tau_0^2$, $\mu'' = 0.722\,88\,\omega\tau_0$, and for $\omega\tau_0 \gg 1$, $\mu' = \mu'' = \delta/R = 0.588\,08(\omega\tau_0)^{-1/2}$; the maximum $\mu''_{max} = 0.377\,45$ occurs at $\omega\tau_0 = 1.093\,75$.

For a bar with rectangular cross section $d\times b$ in parallel ac field one gets from (6.11),

$$\mu(\omega) = 1 - i\omega\tau_0\,\frac{64}{\pi^4}\sum_\mu\sum_\nu \frac{\mu^{-2}\nu^{-2}}{\dfrac{\mu^2+p\,\nu^2}{1+p} + i\omega\tau_0}\,, \tag{8.13}$$

where $p = d^2/b^2$ and $\tau_0 = (\pi^2 D)^{-1}(d^{-2}+b^{-2})^{-1}$, and $\mu,\nu = 1,3,5,\ldots$. In particular, for a bar with square cross section ($p = 1$) one gets

$$\mu(\omega) = 1 - 2i\omega\tau_0\,\frac{64}{\pi^4}\sum_\mu\sum_\nu \frac{\mu^{-2}\nu^{-2}}{\mu^2+2i\omega\tau_0+\nu^2}\,, \tag{8.14}$$

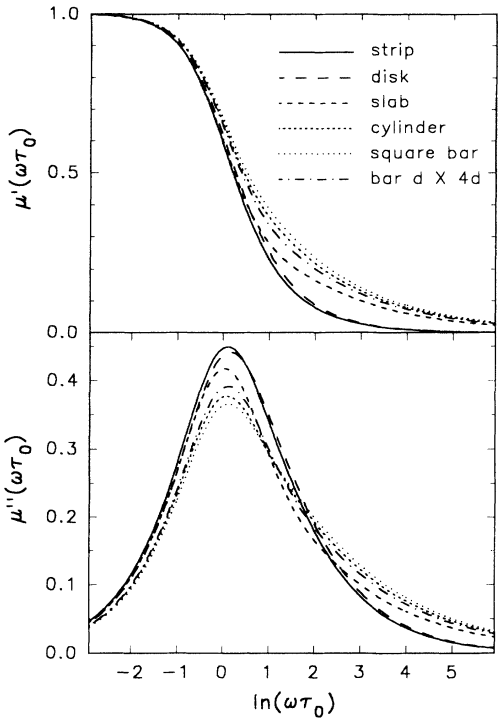

FIG. 12. The ac susceptibility $\mu(\omega) = \mu' - i\mu''$ for various longitudinal geometries (slab, cylinder, square, and rectangular bar) and transversal geometries (strip and disk) plotted on a linear scale versus $\ln(\omega\tau_0)$. Note that with the different τ_0 as time scale (see Table I) the maxima of $\mu''(\omega\tau_0)$ nearly coincide for all geometries.

with $\tau_0 = d^2/(2\pi^2 D)$. For $b \gg d$, Eq. (8.13) can be shown to coincide with the result (8.9) for the slab.

The sum over $\mu,\nu = 1,3,5,\ldots$ in (8.13) converges rapidly and is easily evaluated on a PC. For $\omega\tau_0 \ll 1$ one has for the square bar $\mu'' = 0.693\,720\,\omega\tau_0$ and $\mu' = 1 - 0.663\,360\,\omega^2\tau_0^2$; a maximum $\mu''_{max} = 0.365\,870$

TABLE I. The magnetic response of Ohmic conductors in various geometries: slab, cylinder, bar with square cross section, and bar with side ratio 4 in parallel ac field, and strip and circular disk in perpendicular ac field. Listed are the relaxation time τ_0 (the time unit in this table), the relaxing magnetization $M(t) = c_M M(0)\exp(-t/\tau_0)$ at times $t \gg \tau_0$ after a field change, the real and imaginary parts of the ac susceptibility $\mu(\omega) = \mu' - i\mu''$ at small and large frequencies, and the height and position of the maximum in μ''. The Ohmic (flux flow or TAFF) resistivity ρ determines the flux diffusivity $D = \rho/\mu_0$. Some of the tabulated numbers are given explicitly by $8/\pi^2$, $\pi^4/120$, $\pi^2/12$, $\sqrt{2}/\pi$ (slab); $64/\pi^4$, $2/\pi$ (square bar); $1/2\pi\Lambda_0$, $1/\pi\Lambda_0$, $2/\pi^2\Lambda_0$ (strip, $\Lambda_0 = 0.638\,567\,521$); $1/2\pi\Lambda_0$, $3/2\pi\Lambda_0$, $3/\pi^2\Lambda_0$ (disk, $\Lambda_0 = 0.876\,867$).

		Longitudinal field					Transversal field	
		Slab width d	Cylinder radius R	Square bar $d\times d$	Rect. bar $d\times 4d$		Strip width $2a$	Disk radius a
Relaxation time τ_0		$\frac{d^2/D}{\pi^2}$	$\frac{R^2/D}{5.783}$	$\frac{d^2/D}{2\pi^2}$	$\frac{d^2/D}{1.0625\pi^2}$		$\frac{0.24924ad}{D}$	$\frac{0.18150ad}{D}$
$t \gg \tau_0$	c_M	0.81057	0.69166	0.65702	see text		0.7982	0.7255
$\omega \ll \tau_0^{-1}$	$(1-\mu')/\omega^2\tau_0^2$	0.81174	0.60965	0.66336	0.69783		0.81554	0.75887
	$\mu''/\omega\tau_0$	0.82247	0.72288	0.69372	0.73618		0.85142	0.81134
$\omega \gg \tau_0^{-1}$	$(\omega\tau_0)^{1/2}\mu'$	0.45016	0.58808	0.63662	0.54590	$\omega\tau_0\mu'$	0.49848	0.54451
	$(\omega\tau_0)^{1/2}\mu''$	0.45016	0.58808	0.63662	0.54590	$\omega\tau_0\mu''$	$0.31734\times \ln(10.3\,\omega\tau_0)$	$0.34664\times \ln(9.9\,\omega\tau_0)$
	$\mu''_{max} = \mu''(\omega_{max})$	0.41723	0.37745	0.36587	0.39192		0.4488	0.4411
	$\omega_{max}\tau_0$	1.0295	1.0937	1.1183	1.1139		1.108	1.169

occurs at $\omega\tau_0 = 1.118\,33$. If plotted versus $\omega\tau_0$ where τ_0 is the relaxation time of this geometry, the susceptibilities for all geometries (strip, disk, slab, cylinder, and square and rectangular bars) look qualitatively similar for $\omega\tau_0 < 2$, in particular, all $\mu''(\omega)$ have a maximum of height ≈ 0.40 near $\omega\tau_0 = 1$; cf. Table I and Fig. 12. One might expect that the susceptibility of the cylinder looks similar to that of the square bar, but interestingly, the $\mu(\omega\tau_0)$ of the cylinder and of a rectangular bar with side ratio $b/d = 2.3$ ($p \approx 1/5$) almost coincide (the difference is $< 1\%$). The $\mu(\omega\tau_0)$ of a rectangular bar with $b/d = 4$ approximately falls into the middle between the curves for the square bar ($p = 1$) and the slab ($p = 0$ or $p = \infty$); cf. Figs. 12 and 13 and Table I.

The behavior at $\omega\tau_0 \gg 1$ in general differs for various geometries. Whereas for the slab μ' and μ'' nearly coincide for $\omega\tau_0 \geq 2$, for the cylinder or square bar μ' and μ'' stay different up to rather large frequencies $\omega\tau_0 \approx 50, ..., 200$; cf. Fig. 13. From (8.13) one obtains for rectangular cross section in parallel field at $\omega\tau_0 \gg 1$,

$$\mu(\omega) = \frac{1-i}{(\omega\tau_0)^{1/2}} \frac{(2^{1/2}/\pi)\,(b+d)}{(b^2+d^2)^{1/2}}\,. \tag{8.15}$$

For long bars with arbitrary cross section in parallel field one obtains from (6.16) at large frequencies, with skin depth $\delta_\omega = (2D/\omega)^{1/2}$,

$$\mu(\omega) = \frac{1-i}{2} \frac{\text{surface}}{\text{volume}}\,\delta_\omega\,. \tag{8.16}$$

Remarkably, from the longitudinal susceptibility the ac losses are obtained also in *perpendicular* geometry if the frequency is low enough, $\omega\tau_0 \ll 1$ where τ_0 is the relaxation time of the considered geometry. This is a relatively large frequency range when the specimen is thin. For example, the low-frequency ac losses in a bar, cube, disk, or film with rectangular cross section $d \times b$ and length or thickness L parallel to the field are obtained from (3.16) and (7.15) as

$$P = \omega^2 \rho^{-1} \mu_0^2 \langle H_a(t)^2 \rangle d^3 b\, L\, f(d^2/b^2)\,, \tag{8.17}$$

$$f(p) = \frac{64}{\pi^4} \sum_\mu \sum_\nu \frac{1}{\mu^2\nu^2(\mu^2 + p\nu^2)}\,. \tag{8.18}$$

In particular, for a square bar or square disk one has $b = d$ and $f(1) = 0.035\,144\,29$. For a slab or strip with $b \gg d$ one finds $f(0) = 1/12$; the limit $b \ll d$ decribes the same slab (with x and y interchanged) since $f(p \gg 1) = 1/(12p) = b^2/(12d^2)$.

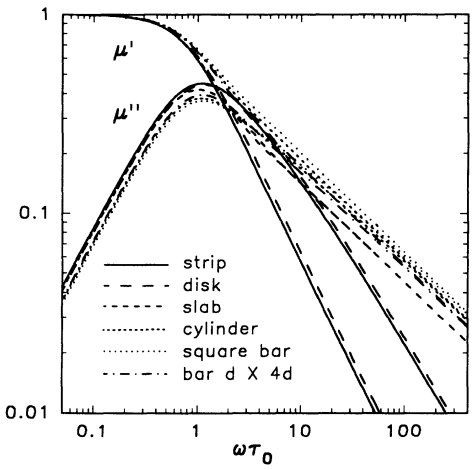

FIG. 13. The ac susceptibility $\mu(\omega) = \mu' - i\mu''$ for various longitudinal and transversal geometries plotted on a log-log scale versus $\omega\tau_0$. Same data as in Fig. 12 and same geometries as in Table I. The asymptotic behavior $\mu' = \mu'' \sim \omega^{-1/2}$ in longitudinal geometry and $\mu' \sim \omega^{-1}$, $\mu'' \sim \omega^{-1}\ln(c\omega)$ in perpendicular geometry is clearly seen in this plot.

IX. DISCUSSION AND SUMMARY

The universal profiles of the sheet current near the edges of thin Ohmic conductors in transversal ac magnetic field [Eqs. (5.7), (5.8), (7.3), and (7.4)] should be compared with the current density profiles near surfaces exposed to a longitudinal ac field; cf. also Eqs. (7.1)–(7.4) of Ref. 1. A switched-on parallel field $H_a(t) = \Theta(t)$ initially penetrates a flat or weakly curved surface of an Ohmic conductor, or a superconductor in the flux flow or thermally assisted flux flow (TAFF) state,[18] *diffusively*, such that the current density $j(\xi,t) = \partial H(\xi,t)/\partial\xi$ is

$$j(\xi,t) = (\pi D t)^{-1/2} \exp(-\xi^2/4Dt) = l^{-1} F_1(\xi/l)\,, \tag{9.1}$$

$$F_1(x) = (2/\pi)^{1/2} \exp(-x^2/2), \qquad l = (2Dt)^{1/2}\,.$$

Here ξ is the spatial coordinate perpendicular to the surface, e.g., $\xi = d/2 - |x|$ for slabs or $\xi = R - r$ for cylinders, and l is the diffusion length with $D = \rho/\mu_0$.

A parallel ac field $H_a(t) = \exp(i\omega t)$ induces a surface current density within the skin depth δ,

$$j(\xi,\omega) = \lambda_{\rm ac}^{-1} \exp(-\xi/\lambda_{\rm ac}) = \delta^{-1} F_2(\xi/\delta)\,, \tag{9.2}$$

$$F_2(x) = (1+i)e^{(1+i)x}, \qquad \delta = (2D/\omega)^{1/2}\,.$$

The universal functions $F_1(x)$ and $F_2(x) = F_2' + iF_2''$ are depicted in Fig. 14 together with the current profile in the Bean critical state, $j(\xi) = j_c$ for $\xi \leq H_a/j_c$ and $j(\xi) = 0$ for $\xi > H_a/j_c$, where j_c is the critical current density. For better comparison, we put $H_a = j_c = l = \delta = 1$ in Fig. 14; all three curves then cover unit area since

$$\int_0^\infty F_1(x)\,dx = \int_0^\infty F_2(x)\,dx = 1\,. \tag{9.3}$$

Thus in longitudinal geometry the total surface current equals the applied field, and the depth of the current carrying layer is $\sim \sqrt{t}$, $\sim 1/\sqrt{\omega}$, or $\sim 1/j_c$. For $t = 0$, $\omega = \infty$, or $j_c = \infty$ the surface current in this idealized picture flows in an infinitely thin layer.

In transversal geometry the current profiles are different. At $t = 0$, $\omega = \infty$, or $j_c = \infty$ the ideal shielding sheet current now depends on the shape of the flat Ohmic conductor; for a strip or disk it is given by $J_0(y)$ (1.4) or $J_0(r)$ (1.5). At finite t, ω, or j_c the infinity of the sheet

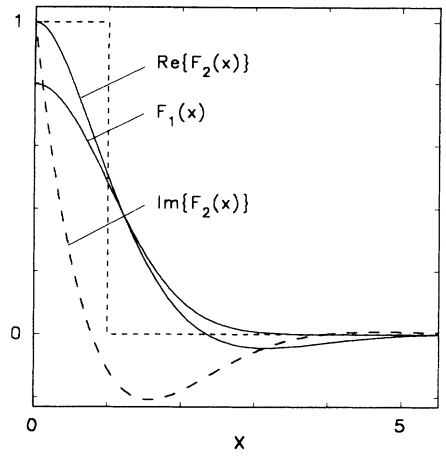

FIG. 14. Self-similarity of the current density near the surface of a long cylinder, slab, or bar in parallel field. At short times after a sudden field change the scaling (9.1) yields the universal profile $F_1(x)$. At large ac frequencies the scaling (9.2) yields the universal profile $F_2(x)$. Real and imaginary parts of F_2 are shown as solid and dashed lines. The rectangular profile (dashed line) gives the current density of the usual Bean critical state; see text. The figure shows how finite time, frequency, or critical current density smear the ideal screening current, which in longitudinal geometry flows in a surface layer of zero thickness (or thickness $\lambda \ll a$).

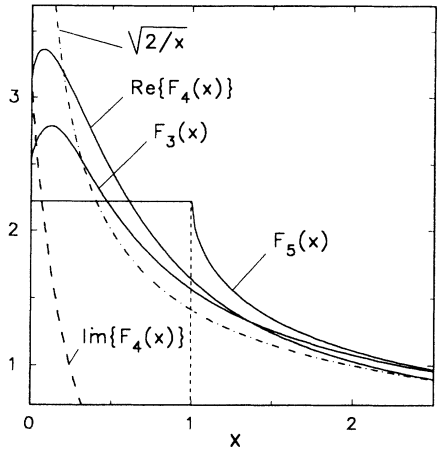

FIG. 15. Self-similarity of the sheet current near the edge of an Ohmic strip or disk, and of thin conductors of arbitrary shape, in perpendicular magnetic field. At short times after a sudden field change the scaling (5.7), (5.8) yields the universal profile $F_3(x)$, Fig. 7. At large ac frequencies the scaling (7.3), (7.4) yield the universal profile $F_4(x)$. Real and imaginary parts of F_4 are shown as solid and dashed lines. The function $F_5(x)$ (9.7) gives the sheet current of the Bean critical state in perpendicular field. The figure shows how finite time, frequency, or critical current density smear the ideal screening current, which is shown as the dash-dotted line $(2/x)^{1/2}$. Note that F_3 and $\mathrm{Re}\{F_4\}$ exhibit a maximum at some distance $x = 0.123$ and $x = 0.074$ from the specimen edge $x = 0$, whereas the corresponding profiles F_1 and $\mathrm{Re}\{F_2\}$ in longitudinal geometry (Fig. 14) have a maximum directly at the specimen surface $x = 0$.

current near the edges is smeared and initially (at small t or large ω) scales according to Eqs. (5.7) and (5.8) or (7.3) and (7.4). The universal current profiles $F_3(x)$ and $F_4(x)$ are shown in Fig. 15 together with the universal profile $F_5(x)$ of the sheet current in the perpendicular Bean critical state occurring near the edge of a superconducting film with constant critical sheet current $J_c = j_c d$.[2-6] The sheet current $J(y)$ in a strip in increasing field H_a is[3-6]

$$J(y) = \begin{cases} \frac{2J_c}{\pi} \arctan \frac{cy}{(b^2 - y^2)^{1/2}}, & |y| < b, \\ J_c\, y/|y|, & b < |y| < a, \end{cases} \tag{9.4}$$

$$c = (1 - b^2/a^2)^{1/2} = \tanh(\pi H_a/J_c)\,. \tag{9.5}$$

For a disk the same expression holds with y replaced by r and with $c = \tanh(2H_a/J_c)$.[2,19,20] Expanding (9.4) for $H_a \ll J_c$ one obtains near the edges of a superconductor strip or disk with constant thickness d (or more generally, with constant J_c) the universal scaling law in increasing field,

$$J(\eta) = J_c \frac{\sqrt{2}}{\pi} F_5\Big(\frac{\eta}{\Delta}\Big)\,, \tag{9.6}$$

with the universal function

$$F_5(x) = \begin{cases} \sqrt{2}\, \arctan(x-1)^{-1/2}, & x \ge 1, \\ \pi/\sqrt{2}, & 0 \le x \le 1, \end{cases} \tag{9.7}$$

and the shape dependent penetration depth

$$\Delta = a - b = \pi^2 H_a^2/2J_c^2 \quad \text{(strip)}, \tag{9.8}$$

$$\Delta = a - b = 2H_a^2/J_c^2 \quad \text{(disk)}. \tag{9.9}$$

Here η is the distance from the edge, $\eta = a - |y|$ or $\eta = a - r$.

The scaling law (9.6) applies to films of arbitrary shape since the prefactor is expressed in terms of J_c. In terms of H_a, the prefactor becomes shape dependent; for the strip one has $J_c\sqrt{2}/\pi = (a/\Delta)^{1/2} H_a$, yielding $J(\eta \gg \Delta) = (2a/\eta)^{1/2} H_a$, and for the disk one gets $J_c\sqrt{2}/\pi = (2/\pi)(a/\Delta)^{1/2} H_a$, yielding $J(\eta \gg \Delta) = (2/\pi)(2a/\eta)^{1/2} H_a$. In Fig. 15 the units are such that the penetration depth $\Delta = 1$ and $H_a = 1$, implying that $J_c = \pi/\sqrt{2}$ for the strip.

All three profiles in Fig. 15 have the same asymptotics, $F_3(x) = F_4(x) = F_5(x) = (2/x)^{1/2}$ for $x \gg 1$, and the areas above and below the ideal-shielding curve $(2/x)^{1/2}$ are equal,

$$\int_0^\infty [F_i(x) - (2/x)^{1/2}]\, dx = 0 \qquad \text{for } i = 3, 4, 5\,. \tag{9.10}$$

Thus, in transversal geometry, finite t, ω, or j_c smear the $x^{-1/2}$ infinity of the sheet current at the specimen edge in a similar and universal way which for weak penetration does not depend on the specimen shape.

The characteristic data of the ac susceptibility $\mu(\omega) =$

$\mu' - i\mu''$ in various geometries are compiled in Table I, namely, the curvature of μ' and slope of μ'' at $\omega = 0$, the asymptotic behavior at large frequencies, and the height and position of the maximum of $\mu''(\omega)$, which determines the maximum possible ac losses (3.16) in a given geometry. Interestingly, the tabulated numbers differ only little for different geometries. The main difference between longitudinal and transversal geometry is the behavior of μ' and μ'' at high frequencies [Eqs. (3.17), (3.18), and (8.16)]. This different asymptotic behavior is clearly seen in the log-log plot of Fig. 13 and may be derived from the short-time relaxation of the magnetization after a field jump, Eqs. (6.16) and (6.1).

An interesting result in parallel ac field is that the complex ac susceptibility of the cylinder (8.12) nearly coincides with that of a rectangular bar (8.13) with cross section $d \times 2.3d$; at large ω the two susceptibilities exactly coincide when the side ratio is $b/d = 2.426\,27\ldots$.

The complex susceptibility of an Ohmic disk with elliptical cross section in transversal field was calculated recently in Refs. 21, 22. These results for the *flat ellipsoid* in general do not agree with the results obtained in the present paper for strips and disks with *constant thickness*, i.e., with a rectangular cross section. At large frequencies, when the skin depth is much smaller than the thickness of the disk, the susceptibility follows from an ideal-screening argument; cf. Sec. II E of Ref. 1 and Eqs. (1.6)–(1.9) above. In this limit the susceptibilities of Refs. 21 and 22 essentially agree with our results (3.17) and (3.18); however, the logarithmic factors are different due to the different cross section. With an elliptic cross section inserted, Eqs. (2.6) and (2.7) or (2.16) and (2.17) reproduce the susceptibility of the flat ellipsoid in Ref. 21. Note that our method is quite general and allows for arbitrary specimen cross section and for arbitrary nonlinear or linear and complex resistivity. For a useful compilation and discussion of various nonlinear susceptibilities derived from the Bean model, see Ref. 23.

If the shape of a thin superconductor or conductor is not an infinite strip or circular disk, one cannot derive one-dimensional integral equations of the type (2.6) and (2.7). In the general transverse geometry one has to resort to a method described in Ref. 24, which requires two-dimensional spatial integration. This spatial integration and the time integration or iteration are performed very efficiently by the matrix method described in this paper. Work on this is under way.

At *low* frequencies, the susceptibility and ac losses of a rectangular disk in transverse field follow from Eqs. (8.17) and (8.18) above. At *high* frequencies, the ideal screening current and the losses in principle may be obtained for any shape of the disk by conformal mapping. From the two limiting expressions at low and high ω the ac losses in the entire frequency range may then be obtained by the interpolation (8.7), which works well in transverse geometry; cf. Fig. 11. An alternative method to obtain $\mu(\omega)$ for arbitrary shape of films or disks is to calculate the relaxation time τ_0 of the magnetization $M(t \gg \tau_0) = c_M M(0) \exp(-t/\tau_0)$ and then insert this τ_0 into the known $\mu(\omega\tau_0)$ for the strip (8.5) and (8.6) or disk (8.3) and (8.4), which differ only little; cf. Fig. 13 and Table I. When expressed as functions of $\omega\tau_0$, the susceptibilities of the disk, strip, square, and rectangle in perpendicular ac field are thus expected to coincide closely.

For Ohmic resistivity ρ, the Maxwell equations describe the diffusion of the current and flux with diffusivity $D = \rho/\mu_0$. In perpendicular geometry, this diffusion becomes *nonlocal* and obeys the integral equations (2.6) (strip) and (2.7) (disk). In the case of nonlinear resistivity $\rho(J)$, these equations describe flux creep in perpendicular geometry. Flux creep in perpendicular geometry may be called nonlinear nonlocal diffusion and has features similar to the usual local but nonlinear diffusion which occurs during flux creep in longitudinal geometry[25,26] and leads to a self-organized critical state. This will be the subject of a forthcoming paper.

ACKNOWLEDGMENTS

I wish to thank Michail Indenbom and Alexander Gurevich and my Stuttgart colleagues for helpful discussions.

APPENDIX A

The functions $p(v)$ (2.5) and $q(v)$ (2.11) may be interpolated and integrated with high precision from a table as follows. First, substitute the variable $v = v(x)$ such that $v(0) = 0$, $v(1) = 1$, $v(2) = \infty$ with $v(x)$ varying smoothly near $v = 0$, $v = 1$, and $v = \infty$. A good such choice is

$$v(x) = [1-(1-x)^4]^2, \quad x(v) = 1-(1-y^{1/2})^{1/4} \quad \text{for } 0 \le x \le 1,\ 0 \le v \le 1, \tag{A1}$$

$$v(x) = [1-(1-x)^4]^{-2}, \quad x(v) = 1+(1-y^{-1/2})^{1/4} \quad \text{for } 1 \le x \le 2,\ 1 \le v \le \infty. \tag{A2}$$

Next, the table $p_i = p[v(x_i)]$ is calculated at equidistant points $x_i = (i-\frac{1}{2})/N$, $i = 1, 2, \ldots, 2N$ ($N \approx 80, \ldots, 200$). Then the function $q[v(x)]$ is tabulated at the same points x_i by direct integration of the table p_i as follows. For $1 \le i \le 6$ (corresponding to small $v \le 484/N^2$) the values $q_i = q[v(x_i)]$ are taken from the expansion (2.12). The remaining q_i for $7 \le i \le 2N$ follow from the recursion

$$q_i v_i = q_{i-1} v_{i-1} - \frac{1}{12} g_{i-2} + \frac{2}{3} g_{i-1} + \frac{5}{12} g_i, \tag{A3}$$

with $g_i = p_i v_i w_i$, $v_i = v(x_i)$, $w_i = v'(x_i)$ (weight function). The sum (A3) calculates the integral

$$q(v) = v^{-1} \int_0^{x(v)} p[v(x)]\, v(x)\, v'(x)\, dx \tag{A4}$$

by approximating the integrand by a parabolic spline. This yields high accuracy in spite of the infinity at $x = v = 1$. For example, with $N = 150$ the relative numerical error of $q(v) = 0.0044\ldots$ at $v = 19$ is 1×10^{-5}.

After this integration is performed, the largest values of the tabulated p_i near $i = N$ ($v \approx 1$) should be reduced, e.g., by multiplying the p_i by a factor

$$[1 - \exp(-\delta_i^2)]^3, \quad \delta_i = \frac{1}{2}\left(N + \frac{1}{2} - i\right), \tag{A5}$$

which replaces $p \approx (1-v)^{-1}$ by $p \approx (1-v)/[(1-v)^2+\epsilon^2]$ with $\epsilon = 32/N^4$. Without this reduction, the extremely large and rapidly varying values $q_i = \pm 8N^4$ for $i = N + \frac{1}{2} \mp \frac{1}{2}$ and $q_i = \pm(8/81)N^4$ for $i = N + \frac{1}{2} \mp \frac{3}{2}$ may lead to noticeable errors in the interpolation procedure when the kernel $P(r,u)$ (2.4) is calculated. This would cause "numerical noise" in the otherwise smooth magnetic field $H(r)$ (2.2). Interestingly, the accuracy of the integration sum (A3) is not affected by the large p_i values; a cutoff which does not conserve the sum over the p_i would rather reduce the accuracy of the q_i.

[1] E. H. Brandt, Phys. Rev. B **49**, 9024 (1994).
[2] P. N. Mikheenko and Yu. E. Kuzovlev, Physica C **204**, 229 (1993).
[3] E. H. Brandt, M. Indenbom, and A. Forkl, Europhys. Lett. **22**, 735 (1993).
[4] W. T. Norris, J. Phys. D **3**, 489 (1970); see also G. W. Swan, J. Math. Phys. **9**, 1308 (1968).
[5] E. H. Brandt and M. Indenbom, Phys. Rev. B **48**, 12893 (1993).
[6] E. Zeldov, J. R. Clem, M. McElfresh, and M. Darwin, Phys. Rev. B **49**, 9802 (1994).
[7] M. Darwin, J. Deak, L. Hou, M. McElfresh, E. Zeldov, J. R. Clem, and M. Indenbom, Phys. Rev. B **48**, 13192 (1993).
[8] D. J. Frankel, J. Appl. Phys. **50**, 5402 (1979).
[9] M. Daeumling and D. C. Larbalestier, Phys. Rev. B **40**, 9350 (1989).
[10] L. W. Connor and A. P. Malozemoff, Phys. Rev. B **43**, 402 (1991).
[11] H. Theuss, A. Forkl, and H. Kronmüller, Physica C **190**, 345 (1992).
[12] M. W. Coffey and J. R. Clem, Phys. Rev. Lett. **67**, 386 (1991); Phys. Rev. B **45**, 9872 (1992); **45**, 10527 (1992); **46**, 11757 (1992); **48**, 342 (1992).
[13] E. H. Brandt, Phys. Rev. Lett. **67**, 2219 (1991); Physica C **185-189**, 270 (1991); **195**, 1 (1992).
[14] E. H. Brandt, Z. Phys. B **80**, 167 (1990).
[15] E. H. Brandt, Phys. Rev. Lett. **68**, 3769 (1992).
[16] R. P. Huebener, L. G. Stafford, and F. E. Aspen, Phys. Rev. B **5**, 3581 (1972).
[17] E. H. Brandt, Phys. Rev. Lett. **71**, 2821 (1993).
[18] P. H. Kes, J. Aarts, J. van den Berg, C. J. van der Beek, and J. A. Mydosh, Supercond. Sci. Technol. **1**, 242 (1989); D. Dew-Hughes, Cryogenics **28**, 674 (1988); E. H. Brandt, J. Supercond. **6**, 201 (1993).
[19] J. Zhu, J. Mester, J. Lockhart, and J. Turneaure, Physica C **212**, 216 (1993).
[20] J. R. Clem and A. Sanchez (unpublished).
[21] E. M. Parvin, A. Singfield, W. F. Vinen, and G. F. Cox, Supercond. Sci. Technol. **6**, 5252 (1993).
[22] M. A. Skvortsov and V. B. Geshkenbein (unpublished).
[23] J. Gilchrist, Physica C **219**, 67 (1994).
[24] E. H. Brandt, Phys. Rev. B **46**, 8628 (1992).
[25] V. M. Vinokur, M. V. Feigel'man, and V. B. Geshkenbein, Phys. Rev. Lett. **47**, 915 (1991).
[26] A. Gurevich and H. Küpfer, Phys. Rev. B **48**, 6477 (1993); A. Gurevich and E. H. Brandt, Phys. Rev. Lett. (to be published).